

Norwegian University of Life Sciences
Faculty of Environmental Sciences
and Natural Resource Management

Philosophiae Doctor (PhD)
Thesis 2022:14

Performance of a photovoltaic-thermal system in a tropical environment of central Ghana

Ytelse av et fotovoltaisk-termisk system
i et tropisk miljø i det sentrale Ghana

Saeed Abdul-Ganiyu

Performance of a photovoltaic-thermal system in a tropical environment of central Ghana

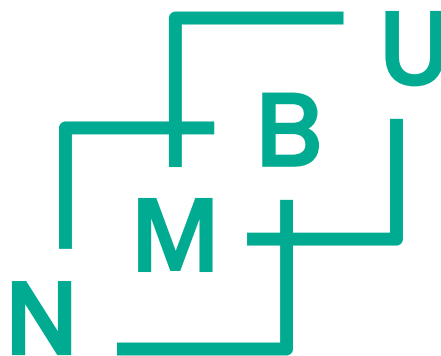
Ytelse av et fotovoltaisk-termisk system i et tropisk miljø i det sentrale Ghana

Philosophiae Doctor (PhD) Thesis

Saeed Abdul-Ganiyu

Norwegian University of Life Sciences
Faculty of Environmental Sciences and Natural Resource Management

Ås (2022)



Thesis number 2022:14
ISSN 1894-6402
ISBN 978-82-575-1862-2

Supervisors and Evaluation Committee

Supervisors

Professor Muyiwa Samuel Adaramola (Main Supervisor)
Renewable Energy Group
Faculty of Environmental Sciences and Natural Resource Management
Norwegian University of Life Sciences (NMBU)
P.O. Box 5003 NMBU, NO-1432 Ås, Norway

Professor Seidu Razak (Co-Supervisor)
Department of Ocean Operations and Civil Engineering
Norwegian University of Science and Technology (NTNU)
Ålesund, Norway

Dr. Emmanuel Wendsongre Ramde (Co-Supervisor)
Senior Lecturer
Department of Mechanical Engineering
Kwame Nkrumah University of Science and Technology (KNUST)
Kumasi, Ghana

Dr. David Ato Quansah (Co-Supervisor)
Senior Lecturer
Department of Mechanical Engineering
Kwame Nkrumah University of Science and Technology (KNUST)
Kumasi, Ghana

Evaluation Committee

Professor Olanrewaju Miracle Oyewola
Fiji National University
School of Mechanical Engineering, Fiji national University, Derrick Campus
Suva, Fiji

Associate Professor Andres Olivares
Western Norway University of Applied Sciences
Bjørnsons Gate 45,
5528 Haugesund, Norway

Professor Kristin Linnerud
Faculty of Environmental Sciences and Natural Resource Management,
NMBU, P.O. Box 5003
1432 Ås, Norway

Acknowledgements

All praises and thanks be to the Almighty God for granting me the resilience to endure whatever life threw at me during this study. The PhD journey has been a true life-changing experience for me, and it would not have been possible without the support and guidance of many individuals and institutions.

I am most grateful to my main supervisor, Prof. Muyiwa Samuel Adaramola for the PhD opportunity in Norway. In fact, there came a time when I almost gave up on the PhD due to some personal setbacks which prolonged the time I spent undertaking my field work in Ghana. Without his guidance, constant support and unwavering ability to drive me back on track, this PhD would not have been achievable. Many thanks also go to my second supervisor, Prof. Seidu Razak, for believing in me by introducing me to Prof. Adaramola which contributed to this PhD fellowship at NMBU. I am also ever grateful for the commitment of his personal time and resources to ensure my comfortable stay in Norway. I lack adequate words to express my profound gratitude to Prof. Seidu for without him, this PhD wouldn't have been possible. I will also like to acknowledge the PhD scholarship support by the UPER-CRET (Upgrading Education and Research Capacity in Renewable Energy Technologies) Program, funded by Energy and Petroleum (EnPe) Project of Norwegian Agency for Development Cooperation (NORAD). I will like to use this opportunity to express my sincere gratitude to the management of NORAD-EnPe.

I am ever grateful to Dr. Emmanuel Ramde for providing the needed technical support and resources to ensure I was always comfortable at KNUST during my time in Ghana for data collection. Special thanks also go to Dr. David Atto Quansah for his brotherliness during our time together in Norway and his subsequent invaluable technical support, encouragements and assistance throughout the challenging times of my PhD journey, right from the beginning to the end of the study. Dr. Ramde and Dr. Quansah formed part of my supervisory team and I deem it an honor to have tapped from their knowledge and expertise. I would also like to express my sincere gratitude to the Brew Hammond Energy Centre, KNUST, for their support in Ghana. I also appreciate the support I got from Professor Ahmed Abdul-Rahman (Current Dean of School of Engineering, KNUST), Dr.

Lena Dzifa Mensah (Dept. of Mechanical Engineering, KNUST) and Mr. Robert Kyere (Technician, Solar Lab, KNUST).

My sincere thanks also go to the Faculty of Environmental Sciences and Natural Resource Management (MINA), NMBU. I would like to mention Dr. Denis Kwame Edem Dzebre for his invaluable assistance of varying forms and for the warmth he extended to me during our time together in Norway and for always making me feel so welcomed. Also, to all former colleagues at MINA (Mekdes, Solrun, Yennie, Thomas and the rest) thanks for your warm friendship. I would also like to thank Mr. Kjetil Sandnes and Volue Instrument Technology Ås (formerly Scanmatic Instrument Technology) for their assistance in purchases and organization of materials for the experimental setup for this thesis. I also thank the Ås muslim community for opening their doors to me. To my family in Ålesund (Fatimat and the kids), I am grateful for the warm reception.

To my wife Salamatu who managed our home in my absence and supportive family, especially my brothers Zakaria and Aminu, I say thank you. To my dad Seidu Sakara who didn't live to see the end of this PhD, God be with you. I will like to thank the entire GOP family (special mention of Harun for IT solutions; also, A. Razak (Zakus), Nurudeen, A. Karim and Ahmed for their constant encouragement), and my friends Mr. Samuel Oyewale and Dr. Isaac Sackey (Berlin).

Finally, and most importantly, I wish to once again express my sincere gratitude to the Almighty God for the success of this PhD has not been by my strength, but by His will for my life.

Alhamdulillah

Table of Contents

Supervisors and Evaluation Committee	2
Acknowledgements	3
Abbreviations and definitions.....	6
List of papers	10
Abstract	11
Norsk Sammendrag.....	13
Synopsis.....	15
1 Introduction	16
2 Fundamental theory of modules	24
3 Materials and Methods	44
4 Results and discussion	60
5 Conclusions	66
6 Limitations of work, future studies and engineering direction.	68
References.....	70
7 Articles/Papers	77
I Investigation of Solar Photovoltaic-Thermal (PVT) and Solar Photovoltaic (PV) Performance: A Case Study in Ghana	
II Techno-economic analysis of solar photovoltaic (PV) and solar photovoltaic thermal (PVT) systems using exergy analysis	
III Study Effect of flow rate on flat-plate water-based Photovoltaic-Thermal (PVT) system performance by analytical technique	
8 Appendices	

Abbreviations and definitions

English letters

A_m	Effective module surface area (m^2)
A_{th}	Area of thermal collector
A_x	surface x, where x is a positive integer
b	Economic life of the system (years)
C_1	A constant = $2\pi hS_o^2 = 3.74177 \times 10^8 \text{ W } \mu\text{m}^4/\text{m}^2$
C_2	A constant = $hS_o/k = 1.43878 \times 10^4 \mu\text{m K}$
C_b	Conductance of the bond between the fin and copper circular pipes
C_t	Total cost (\$)
c_p	Specific heat capacity of water ($\text{kJ}/\text{kg } ^\circ\text{C}$)
d	Characteristic linear dimension in m
d_p	The thickness of the pottant
D	External diameter of the pipes
D_i	Internal diameter of the pipes
E_{BG}	Band-gap energy
$E_{c.el}$	Electrical energy generated by cell, per unit area
$E_{c.th}$	Thermal energy generated by cell, per unit area
$E_{c.th-p}$	Transfer of thermal energy, per unit area, from the cell to the thermal plate
$E_{c.l}$	Solar cell energy losses per unit area
E_{dc}	DC electrical power (W)
E_{g-c}	Energy, per unit area from glass to solar cell
E_{g-p}	Energy per unit area due to insolation incident between the cells to pottant
$E_{g,l-a}$	Net energy per unit area from the glass to ambient
E_n	Electric valve n, where n is an integer
E_{PH}	Photo energy
E_{th}	Useful thermal power gain (W)
EX_{el}	Electrical exergy in (kWh)
EX_{th}	Thermal exergy in (kWh)
EX_{out}	Net exergy output of PVT system in (kWh)
$EX_{pvt,t}$	Annual exergy from the system in year t in (kWh)
f	frequency
F	Efficiency factor
F_{12}	View factor of surface 2 from 1
F_c	Collector efficiency factor
FF	Fill factor
F_R	Heat removal factor
G_p	In-plane irradiance in (W/m^2)
h	Plank's constant
h_c	Convection heat transfer coefficient
h_{fi}	Heat-transfer coefficient of the fluid
h_r	Radiation heat transfer coefficient
$h_{c,g-a}$	Convective heat transfer coefficient from glass to ambient.
$h_{r,c-g}$	Radiation heat transfer coefficient from cell to glass
h_w	Wind heat transfer coefficient ($\text{W}/\text{m}^2 \text{ } ^\circ\text{C}$)

I_O	Reverse bias (or dark) saturation current
I_{bat_t}	The installed cost (\$) of battery in year t
I_D	Diode or dark current
I_{MPP}	Current at MPP
I_{ph}	Photocurrent
I_{SC}	Short circuit current
I_t	Total investment expenditure in year t
I_{inv_t}	The installed cost (\$) of inverter in year t
J	Radiosity
$k_c,$	Thermal conductivity
k	Boltzmann constant (given as 1.602×10^{19} J/V)
k_b	Back insulation conductivity
k_f	Thermal conductivity of the fluid in W/m K
k_g	Cover glass thermal conductivity
k_p	Coefficient of thermal conductivity of the pottant
k_{th}	Absorber thermal conductivity
L	Representative dimension
L_b	Back insulation thickness
L_e	Edge insulation thickness
l_g	Cover glass thickness
L_t	Financial loan cost in year t
l_{th}	Absorber thickness
$LCOE$	Levelized Cost of Energy
$LCOEx$	Levelized Cost of Exergy
\dot{m}	Mean mass flow rate
m_w	Mass flowrate of water
M_t or $O\&M$	Operation and maintenance cost (\$)
N	Number of glass covers
n	Ideality factor ranging from 1(ideal) to 2
N_u	Convection heat transfer coefficient
NPV	Net present value
P	Power
p	Parking factor of the cell
P_b	Total emissive power of blackbody
P_{bx}	Total emissive power from blackbody x, where x is a positive integer
P_e	Real surface emissive power
$P_{b\lambda}$	Monochromatic emissive power
P_r	Prandtl number
P_{MPP}	Maximum power point
PV_{CF}	Present value of the cash flow (\$)
PV_{Ex}	Present value of the exergy (W)
q	Electron charge (1.381×10^{23} J/K)
Q_{12}	Net radiation exchange between surfaces 1 and 2
Q_u	Useful thermal energy
r	Discount rate (%)
r_i	The refraction index of the medium
R	Collector perimeter
Re	Reynolds number

R_S	Series resistor
R_{SH}	Shunt resistor
S	Speed of light ($S_o \approx 300,000$ km/s in a vacuum)
Sp_t	Total support and incentives in year t (\$)
t	Time in years
T	Absolute temperature
T_1 or T_i	Water inlet temperature in °C
T_2 or T_c	PVT cells back temperature in °C
T_3 or T_o	Water output temperature in °C
T_4 or T_c	PV cells back temperature in °C
T_5	Reservoir water temperature in °C
T_a	Ambient temperature in °C
$T_{a.min}$	Minimum ambient temperature
\dot{T}_c	Mean temperature for cell
\dot{T}_g	Mean temperature for glass
T_p	Absorber plate surface temperature
\dot{T}_p	Average plate temperature
T_{ref}	Reference temperature in °C
Tx_t	Total tax paid in year t (\$)
T_{sky}	Sky temperature
U_b	Back loss coefficient
U_e	Edge loss coefficient.
U_t	Top loss coefficients
U_L	Overall losses coefficient
v	The fluid flow rate
V	Voltage
V_D	Diode voltage
V_{MPP}	Voltage at MPP
V_n	Manual valve n, where n is an integer
V_{oc}	Open circuit voltage
V_T	Thermal voltage
W	Pipe spacing
w	Wind speed in m/s

Greek letters

α	Absorptivity
α_c	absorptance of the solar cell
α_g	cover glass absorptance
β	temperature dependent coefficient of electrical efficiency
ε	Emissivity
ε_c	emissivity for cell
ε_g	emittance of cover glass
ε_{th}	emittance of thermal absorber
ε_{ϑ}	temperature coefficient of parameter ϑ
η_0	efficiency at standard test conditions (STC)
η_{el}	Module electrical efficiency (%)
η_{ex}	Overall exergy efficiency (%)
η_{PVT}	Total efficiency of the PVT (%)

η_{th}	Module's thermal efficiency (%)
ϑ_{T_c}	parameter value at cell temperature T_c
$\vartheta_{T_{ref}}$	parameter value at reference temperature T_{ref}
θ	collector tilt (deg)
τ_g	glass transmittance
λ	wavelength
ρ	reflectivity
ρ_g	reflectivity of the glass
σ	Stefan–Boltzmann constant = $5.6697 \times 10^{-8} \text{ W/m K}^4$
τ	transmissivity
τ_g	Transmittance of glass
τ_p	Transmittance of pottant
ω	dynamic viscosity in pascals

Abbreviations

AIST	Japan National Institute of Advanced Industrial Science and Technology
BOS	Balance-of-system
CCT	Control circuit
CIS	Copper Indium Selenium
CdTe	Cadmium telluride
CO ₂	Carbon dioxide
DC or dc	Direct current
EnPe	Energy and Petroleum
FHG-ISE	Fraunhofer Institut für Solare Energiesysteme
IEA	International Energy Agency
IRENA	International Renewable Energy Agency
KNUST	Kwame Nkrumah University of Science and Technology
mc-Si	Mono-crystalline silicon
MINA	Faculty of Environmental Sciences and Natural Resource Management
MPPT	Maximum Power Point
NMBU	Norges miljø- og biovitenskapelige universitet (Norwegian University of Life Sciences)
NORAD	Norwegian Agency for Development Cooperation
NREL	National Renewable Energy Laboratory
Pt 100	Platinum temperature transducer
PV	Photovoltaic
PV_Bat	Photovoltaic Battery
PVT	Photovoltaic-thermal
PVT_Bat	Photovoltaic-thermal battery
RH	Relative humidity
SDG	Sustainable Development Goal
SE4ALL	Sustainable Energy for All
STC	Standard Test Condition (which are defined as Irradiance = 1000 W/m^2 , $T_c = 25 \text{ }^\circ\text{C}$, and air-mass ratio = 1.5)
UPER-CRET	Upgrading Education and Research Capacity in Renewable Energy Technologies
WHO	World Health Organization

List of papers

-
- Paper 1** **Saeed Abdul-Ganiyu**, David A. Quansah, Emmanuel W. Ramde, Razak Seidu and Muiyiwa S. Adaramola (2020). Investigation of Solar Photovoltaic-Thermal (PVT) and Solar Photovoltaic (PV) Performance: A Case Study in Ghana. *Energies*, Volume 13 (11), May 2020, 2701; <https://doi.org/10.3390/en13112701>
- Paper 2** **Saeed Abdul-Ganiyu**, David A. Quansah, Emmanuel W. Ramde, Razak Seidu and Muiyiwa S. Adaramola (2021). Techno-economic analysis of solar photovoltaic (PV) and solar photovoltaic thermal (PVT) systems using exergy analysis. *Sustainable Energy Technologies and Assessments*, Volume 47, October 2021, 101520; <https://doi.org/10.1016/j.seta.2021.101520>
- Paper 3** **Saeed Abdul-Ganiyu**, David A. Quansah, Emmanuel W. Ramde, Razak Seidu and Muiyiwa S. Adaramola. Study Effect of flow rate on flat-plate water-based Photovoltaic-Thermal (PVT) system performance by analytical technique. *Journal of Cleaner Production*, Volume 321, September 2021, 128985; <https://doi.org/10.1016/j.jclepro.2021.128985>
-

Abstract

Access to energy has been heavily linked to socio-economic development. It is therefore not surprising that the energy poverty in sub-Saharan Africa has affected development in the subregion. However, as development increasingly becomes emissions-constrained, the role of renewable technologies takes on added significance and urgency. Thus, in the case of Sub-Saharan Africa, solar energy technologies come in handy in reducing the energy deficit while addressing emissions concerns. One innovative solar technology that combines conventional PV and solar thermal systems into one is the photovoltaic-thermal (PVT) technology. Although the PVT technology is seen to have a lot of potential in providing remote solutions, its performance is heavily linked to the environment where it is deployed. Nonetheless, the PVT technology has not been commercially successful as the conventional systems due to many reasons including lack of information and standards about the technology. Also, the PVT technology requires higher initial capital costs compared to separate solar PV and thermal systems – raising the question of whether it is really worth such investments.

Investment decision on the other hand relies on data regarding expected system performance in the deployed environment. While the PVT technology has been investigated in many places in the world, little can be said about field data on the technology in sub-Saharan Africa. The aim of this thesis is thus to scientifically contribute to bridging the data under-representation from countries in Africa in the area of PVT by assessing the technology in a tropical environment of Ghana.

To that end, an experimental setup comprising a water-based mono-crystalline PVT and a conventional mono-crystalline PV is installed at the Kwame Nkrumah University of Science and Technology in Kumasi and its short to long term performance assessed. The results for the study were communicated in three journal articles (Papers 1, 2 and 3).

Paper 1 assessed the real-life outdoor technical performance of the PVT module against a conventional PV system in a hot humid tropical climate in Ghana. Whereas the highest monthly mean efficiency recorded for the PV was 12.7%, the highest combined measured monthly mean electrical/thermal efficiency of the PVT was 56.1%. Based on their technical performances, it was concluded that the PVT is a worthy prospective alternative

energy source in off-grid situations, especially when both electrical and thermal energies are desired.

Paper 2 investigated the long term technical and economic viability of the PVT module in comparison with the conventional PV over a 25 year-period. It was observed that whereas it required about twice the upfront-cost for the PV-system/m² to setup the PVT-system/m², the battery cost accounted for about 61% and 34% of life cycle cost for PV and PVT systems respectively. Nonetheless, the PVT generally performed better than the PV in stand-alone situations when installed with batteries as back-up. However, the PV system becomes more economically viable than the PVT system when both systems were installed without batteries.

Paper 3 focused on the effect of flowrate on the performance optimization of the PVT system. The optimal flowrate for the PVT was observed to be 0.063 kg/s m². It was concluded that the commercial PVT system did not perform as expected in exergy terms when compared with separately installed conventional PV and thermal systems. The use of exergy at various mass flowrates and irradiances showed that using only combined efficiency, which is widely used approach, is not enough to assess PVT general performance.

In terms of degradation, it was generally concluded that the rate of degradation of output exergy due to ageing was projected to be lower in the commercial PVT module than the conventional PV module. This has been estimated to reach 11.3 % and 12.8 % respectively for the PVT and PV modules in their estimated 25-year economic life, which translates into approximately 6.1 % of total exergy losses for each module over the period. In addition, whereas the output losses of the PVT system increased curvilinearly from 15.4% to 26.7% over its economic life, that of the PV system increased from 16.1% to 31.7%.

Norsk Sammendrag

Tilgang til energi har stor korrelasjon med sosioøkonomisk utvikling. Derfor er det ikke overraskende at energifattigdom i Afrika sør for Sahara har påvirket økonomisk utviklingen i subregionen. Ettersom utviklingen i økende grad blir utslippsbegrenset, får fornybar teknologis rolle større betydning. I Afrika sør for Sahara, kommer solenergiteknologier til nytte for å redusere energiunderskuddet og utslippsproblemer. En innovativ solteknologi kombinerer konvensjonelt PV-system og sol termisk system til fotovoltaisk-termisk teknologi (PVT). Selv om PVT -teknologien har et stort potensial særlig i landlige områder, er ytelsen sterkt knyttet til miljøet der den er installert. PVT-teknologien har ikke vært kommersielt vellykket sammenlignet med de konvensjonelle systemene på grunn av mange årsaker, som mangel på informasjon og standarder til teknologien. PVT -teknologien krever også høyere startkapitalkostnader sammenlignet med separate solcelle -PV- og termiske systemer. Her kan man stille spørsmålet om det virkelig er verdt slike investeringer. Investeringsbeslutning er på den annen side avhengig av data om forventet systemytelse i det miljøet hvor systemet er installert.

Selv om PVT-teknologien har blitt undersøkt mange steder i verden, kan lite sies om feltdata om teknologien i Afrika sør for Sahara. Målet med denne oppgaven er å bidra til å bygge bro over datagapet ved å vurdere ytelsen til en PVT i et tropisk miljø i Ghana. For dette formål er et eksperimentelt oppsett som består av en vannbasert monokrystallinsk PVT og en konvensjonell monokrystallinsk PV installert ved Kwame Nkrumah University of Science and Technology i Kumasi, og dens korte til langsiktige ytelse vurderes. Resultatene for studien ble presenterte i tre tidsskriftartikler (1, 2 og 3).

I Artikkel 1 ble den virkelige utendørs ytelsen til PVT-modulen vurdert opp mot et konvensjonelt PV-system i et varmt fuktig tropisk klima i Ghana. Resultatene viser at den høyeste målte månedlige gjennomsnittlige effektiviteten for PV var 12,7%, mens den høyeste målte månedlige gjennomsnittlige elektriske / termiske effektiviteten til PVT var 56,1%. Det ble konkludert med at PVT er en verdig potensiell alternativ energikilde i områder utenfor strømmettet.

Artikkel 2 undersøkte den langsiktige tekniske og økonomiske levedyktigheten til PVT-modulen i sammenligning med den konvensjonelle PV-en over en 25-års periode. Resultatene viste at mens det krevde omtrent to ganger den opprinnelige kostnaden for å sette opp PV-systemet/m² enn for å sette opp PVT-systemet/m², var batterikostnaden omtrent 61% og 34% av livssyklus-kostnadene for henholdsvis PV- og PVT-systemer. Generelt fungerte PVT systemet bedre enn PV i frittstående situasjoner installert med batterier. PV -systemet blir imidlertid mer økonomisk levedyktig enn PVT -systemet når begge systemene ble installert uten batterier.

Artikkel 3 fokuserte på effekten av vannstrømningshastighet på ytelsesoptimaliseringen av PVT -systemet. Resultatene viste at den optimale strømningshastigheten for PVT var 0,063 kg/s m². Det ble konkludert med at det kommersielle PVT -systemet ikke fungerte som forventet med tanke på energi sammenlignet med separat installerte konvensjonelle PV- og termiske systemer. Bruken av eksergi ved forskjellige massestrømningshastigheter og bestrålinger viste at det ikke er nok å bruke bare kombinert effektivitet, som er mye brukt, for å vurdere dens generelle ytelse.

Når det gjelder nedbrytning, ble det generelt konkludert med at nedbrytningshastigheten for utgående eksergi på grunn av aldring anslås å være lavere i den kommersielle PVT -modulen enn i den konvensjonelle PV-modulen. Dette har blitt estimert til å nå henholdsvis 11,3 % og 12,8 % for PVT- og PV -modulene i deres estimerte økonomiske levetid på 25 år, noe som gir omtrent 6,1 % av de totale eksergitapene for hver modul over perioden. Mens energitapene til PVT -systemet økte krumlinjært fra 15,4% til 26,7% i løpet av dets økonomiske levetid, økte energitapene til PV systemet fra 16.1% til 31.7%.

Synopsis

1 Introduction

1.1 Energy and socio-economic development

Socio-economic development across the globe is linked to the availability of reliable energy. Meanwhile, billions of people worldwide do not have access to electricity, clean cooking and space heating [1] and are trapped extensively in a vicious cycle of poverty. The situation is particularly dire in Africa, which is home to 17% of the world's population but generates only 4% of global power supply [2]. Indeed, efforts to promote electrification are gaining momentum on the continent but are far outpaced by rapid population growth. As of 2019, the electrification rate in sub-Saharan Africa was 47.9% [2] with frequent electricity disruptions and economic losses. The corollary of this is that four out of five people in sub-Saharan Africa rely on the use of environmentally unsustainable energy sources such as fuel wood, mainly for heating water and cooking food resulting in deforestation and pulmonary diseases. Apart from the environmental impacts, these energy sources have been associated with significant health risks. According to World Health Organization (WHO), household air pollution from cooking with traditional solid fuels contributes to between three and four million premature deaths every year, globally [3]; this exceeds deaths due to malaria [4] and tuberculosis [5] combined.

Africa is experiencing a rapid urbanization coupled with increased development of small, medium and large-scale businesses. It is therefore anticipated that the overall demand for energy will continue to expand in Africa, as increasing prosperity in fast-growing urban economies lifts millions of people from poverty [6]. The growing energy demand poses a significant challenge- how to meet Africa' increasing energy demand as it grows and prospers while also reducing carbon emissions.

Carbon emission is projected to grow an average of 0.6 % per year between 2015 and 2040 [7]. Concerns emanating from global warming, Carbon dioxide (CO₂) emissions, depleting fossil fuel reserves have become topical issues in the current global energy scenario [8] [9]. As a result, 195 countries adopted the first-ever universal, legally binding global climate deal in Paris in December 2015 [10] [11]. The agreement sets out a global action plan to put the world on track to reducing the impacts of climate change by limiting

global warming to well below 2°C [10]. The International Energy Agency's (IEA) 450 Scenario suggests that carbon emissions need to fall by around 30% by 2035 to have a good chance of achieving the goals set out in Paris [6]. There is therefore a need to cut down on fossil fuel as sources of energy for cleaner and sustainable sources. Although energy-related CO₂ emissions remained stable in 2019, largely due to economic downturn as a result of the global COVID-19 pandemic, the world is not on track to limit global warming to well below 2°C as stipulated in the Paris Agreement [12].

The global energy poverty challenge has therefore become one in which both socio-economic development and reduction in global greenhouse gas emissions are pursued concurrently [13]. The United Nation's Sustainable Energy for All (SE4ALL) program is an example of many global initiatives that attempt to demonstrate the feasibility of pursuing these multiple goals without controversy. The SE4ALL initiative presents a nexus between energy access and climate change, and environmental sustainability more broadly - to mobilize various stakeholders to achieve universal access to modern energy services, doubling the share of renewable energy in the global energy mix and doubling the rate of improvement in energy efficiency, all by 2030 [13].

1.2 Renewable Energy Trends and Technologies in sub-Saharan Africa

Renewable energy global power share is estimated to increase from 7% in 2015 to nearly 20% by 2035 [6]. The importance of renewable sources to the global energy order is highlighted in the era of the novel global COVID-19 pandemic. The exogenous impact of the pandemic on global economic slowdown and its adverse effect on energy demand had little influence on the growth of renewables in power generation. In 2019, renewables were the only source of electricity to record demand growth over this period, due to low operating costs and preferential access to electricity networks [12]. Nonetheless, the stated reasons may not constitute a global representation of the situation in its entirety.

Expanding renewable energy access in Africa, for instance, will not only reduce poverty and greenhouse gases but will also improve gender equality and sanitation on the continent [14]. Apart from energy provision, renewable technology has the potential to reduce the continent's employment deficits. However, a recent IRENA (International Renewable Energy Agency) report shows that less than 2 % of 11 million renewable-

energy jobs created globally is in sub-Saharan Africa [15]. These and many more have hampered industrial expansion on the continent and access to quality life, making it the poorest continent on the globe.

Among the renewable energy technologies that exist today, those based on solar energy has greatest potential in meeting the growing energy needs in Africa since it is an abundant and essentially inexhaustible source of energy accessible [8]. Africa has the richest solar resources in the world, but accounts for less than 1% of global solar PV installed capacity [2] mainly due to lack of favorable renewable energy policies such as those advancing affordability. Solar resources provide the option of decentralized (and off-grid) solutions to remote settlements because they are more reliable and much quicker to deploy. For example, the number of people who gained access to electricity through solar home systems in sub-Saharan Africa increased from two million in 2016 to approximately five million in 2018 [2].

Solar energy is commonly exploited through two main mechanisms, which are heat energy (for solar thermal systems) and light energy (solar photovoltaic systems). A hybrid photovoltaic-thermal (PVT) system combined these two mechanisms together as a single system. The solar PV component generates electricity while the integrated thermal absorber collects useful heat energy from the solar PV, reducing the solar PV cells temperature and thus, enhance their efficiency [16] [17]. Figure 1.1 shows an elaborate classification of PVT.

Hybrid PVT collectors are capable of reaching net (electrical plus thermal) efficiencies of 70% or higher, with electrical efficiencies up to 15–20% and thermal efficiencies in excess of 50%, depending on the conditions [18]. The combination of two technologies in one module also has the potential to reduce the use of materials, the time of installation, and the required space [19].

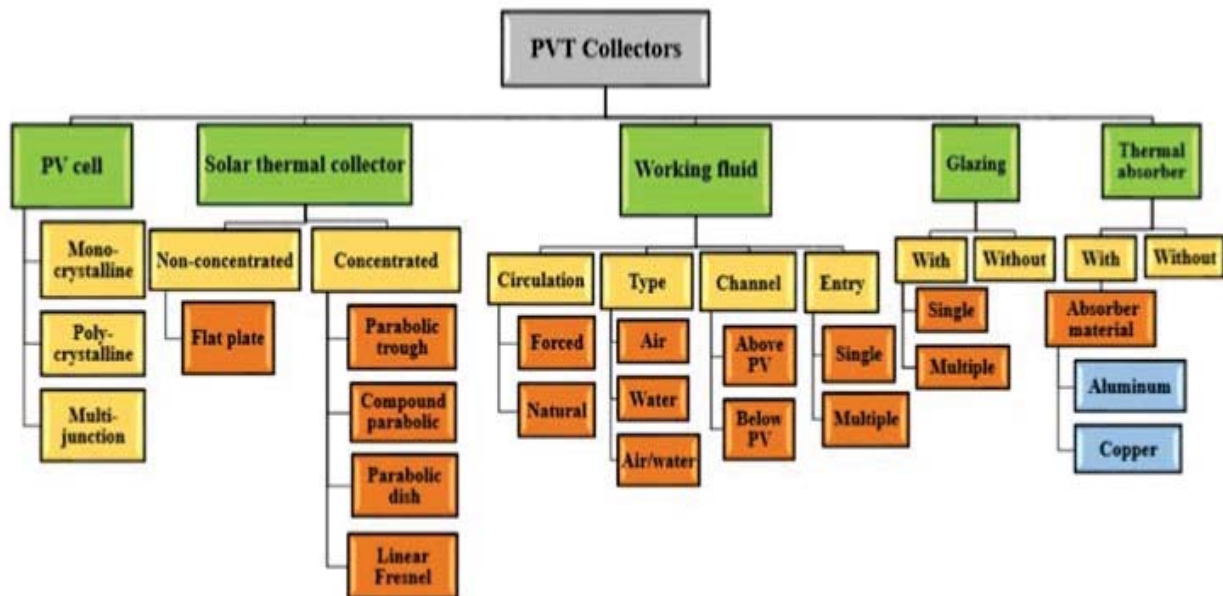


Figure 1.1: Classification of PVT solar collectors [20]

Ghana is in the tropical region of sub-Saharan Africa with relatively high ambient temperature and low wind speeds. Quansah et al. [21] have shown that solar PV systems installed in this region generally have higher module temperatures, which lead to power losses and hence, relative low performance ratios. This raises a concern about how to reduce PV modules temperature and thereby, improve their performance, and also harness the heat energy for potential users in the said environment. The PVT technology serves both purposes and hence the basis to investigate it in comparison with the PV technology in the said environment.

The advantages of the PVT system in generating electricity and simultaneously extracting the heat generated for useful means are suitable for residential applications. However, despite the potential of PVT systems, commercial PVT systems are still not as popular as stand-alone, and separately installed, PV and Thermal systems [22]. However, the deployment of stand-alone solar PVT technology requires higher initial capital costs - compared to separate solar PV and thermal systems - raising the question of whether it is really worth such investments. This could be ascertained scientifically by investigating its overall life cycle performance in the economic environment it is to be deployed. Investment due-diligence requires an understanding of the risk-return profiles to facilitate informed decisions. Therefore, this study will also seek to understand the economic feasibility of the PVT technology in comparison with the conventional PV

system in the economic environment of Ghana.

1.3 Problem Statement

PVT technologies have been studied since 1970s, including variation in designs, working fluids and other performance-influencing factors [17, 23]. The thermal and electric energy outputs depend on many factors, some of which are irradiance, ambient temperature, wind speed, circulating fluid temperature and flowrate [24, 25, 26]. Unlike indoor test conditions, climatic conditions could vary significantly affecting general performance and resilience of designs. For instance, the harsh harmattan weather conditions of sub-Saharan West Africa set it apart from other places in the world.

Two key factors to assess PVT system performance and technical characterization are the climatic conditions [27] and the operation temperature [28]. However, several of the experimental studies to predict the performance of PVTs were carried out in Europe (e.g. Spain [24], Cyprus [25] [29], Netherlands [30], France/Germany [31] and Greece [32]) and many parts of Asia (e.g. Malaysia [33], Taiwan [34], Hongkong [35], and China [36] [37]) with minimal experimental investigation records on the subject in sub-Saharan Africa in open literature. The few studies on PVT technology in Africa in the literature are based on climates of North Africa sub-region [26] [38] [39] and the country of South Africa [39] [40] [41] [42]. In the case of West Africa, studies on solar technology are either separately conducted on solar photovoltaic systems (e.g. [43] [44] [45] [46] [47] [48]) or solar thermal systems [48] [49] [50] [51], with very little evidence of studies on performance of the combined technology (PVT) in the literature. Like Aste et al. [27], Rajoria et al. [8] have also shown that PVT systems performance is directly related to climatic conditions. Thus, a performance assessment in the intended environment of deployment is necessary to make informed decisions on the technology.

In the case of economic performance, comparative techno-economic analyses of energy from flat-plate water PVT and conventional PV systems have been undertaken by a few authors from various locations worldwide. Herrando et al. [52] developed a model to assess the suitability of hybrid PVT systems for the provision of electricity and hot water in a domestic household in the temperate United Kingdom environment. They studied

the influence of varying collector flowrate and the covering factor of the solar collector with PV. They concluded that, with respect to primary energy and decarbonization, the PVT systems offered significantly improved proposition over equivalent conventional PV-only systems, but at a higher cost. In a further study, Herrando and Markides [53] considered the economic aspects based on which invaluable policy-related conclusion were drawn concerning the influence incentives including a proposed Renewable Heat Incentives. In addition to previous conclusions [52], they opined that although domestic heating demands in the UK outweighs electricity consumption by a factor of about 4, the support landscape strongly favoured electricity microgeneration which in turn favours PV only technology. Kalogirou and Tripanagnostopoulos [32] investigated the industrial application of PVT systems, relative to conventional PV systems. They proved the economic viability of the systems by showing that positive life cycle savings are obtained in the case of PVT systems compared with the PV, and the savings increased for higher load temperature applications. In another study [54], Tselepis and Tripanagnostopoulos undertook a cost/benefit analysis of PVT systems, and compared the payback time with separately installed conventional PV and solar thermal under support schemes and conditions in Greece.

The aforementioned comparative economic feasibility studies for the conventional PV and PVT ([52], [53], [32], [54]) were all based on energy analysis. Both electrical and heat are of different thermodynamic energy qualities and hence not comparable. Whereas energy is a conserved quantity based on the first law of thermodynamics, exergy is not conserved and is based on the second law of thermodynamics. Thus, exergy analysis allows qualitative assessment by comparing electrical and thermal energy based on the same standard and thus serves as a better parameter for comparing the two energies. Secondly, different pricing regimes and uneven incentive policies for heat and electrical energy in different economies could affect results for different regions. Thirdly, the study by Kalogirou and Tripanagnostopoulos [32] was skewed towards achieving higher heat energy for industrial application at the expense of electrical energy. Thus, flowrate analysis to achieve optimal overall performance for the PVT was not considered. Such a setup may affect the overall efficiency of the PVT.

Ghana has an all-year and near-uniform solar resource of average daily peak sun hours of 5.1 h [55] (see Appendix A), but like most countries in West Africa, water heating is mostly by either biomass, natural gas or electrical heaters with minimal use of solar options. Notwithstanding, the commercialization of PVT technology has generally not been successful [24] as the separate conventional PV and solar heaters. According to the IEA (Task 60), this is largely due to lack of information about the possibilities and benefits of PVT solutions, and the lack of international standards, which creates less confidence for end users [56]. These and many more have necessitated the need for a regional (or climate) based investigation of the PVT technology.

1.4 Aim and objectives of the thesis

Based on the aforementioned, the overall aim of this thesis is to assess the performance of a PVT in a tropical environment of Ghana. The specific objectives are:

1. To evaluate the technical performance of a flat plate water PVT system in comparison with a conventional system (Paper 1).
2. To assess life time cost effectiveness of flat plate water PVT system using exergy analysis as an economic parameter (Paper 2).
3. To assess the effect of flowrate on the performance optimization of flat plate water PVT system against the conventional PV system (Paper 3).

1.5 Contribution and Significance of Study

It is expected that the results of this study will contribute to the general body of knowledge. The study explores the use of exergy as an economic parameter in assessing the long-term feasibility of the PVT system in comparison with conventional systems. Secondly, this thesis is also expected to contribute to efforts at addressing issues of data under-representation from countries in Africa in the area of PVT technology. Thirdly, this thesis will be beneficial to stakeholders in making informed decision with regards to the options available to them in the use of solar technology. Residential and hospitality industry could significantly benefit hugely from reduced water heating and electricity bills through the use of PVT systems. Lastly, the findings of this study are expected to be directly beneficial to Sustainable Development Goal (SDG) 7, which is affordable and clean energy, and indirectly to other SDGs, such as SDG 3 (good health and well-being), SDG 11 (sustainable cities and communities), and SDG 13 (climate action).

1.6 Organization and structure of the Thesis

The thesis is based on three papers and generally structured into five sections. The first section introduces the topic, the problem statement and also presents the main aim and objectives of the study. The second section presents the fundamental theory underpinning the operation of the PV and PVT modules used for the study. Section three deals with the research methodology which details the experimental setup, analytical models and techniques to process information collected from the setup. Section four presents the main findings following the analysis of data from the experiment aimed at addressing the main objectives of the thesis. The fifth section presents a summary of the major conclusions of the entire study. The final section looks into limitations of the work and recommends practicable engineering directions based on findings as well as perspectives for further research.

2 Fundamental theory of modules

This section explains the theories behind the general solar energy conversions by the PV and PVT modules used in this thesis. It begins with the fundamental theory of photovoltaic cells. The general physics of heat transfers between materials is then addressed. This is followed by theory of operation of water flat plate thermal collectors. Finally, the analytical models for thermal energy transfer across the PVT are presented.

2.1 Fundamental theory of photovoltaic cells

The solar PV cell is a solid-state device which converts sunlight, as a stream of photons, into electrical power. The working principle of solar cells is based on the photovoltaic effect, that is, the generation of a potential difference at the junction of two different materials in response to electromagnetic radiation. For an absorbed photon to cause a photovoltaic effect in a semiconductor, its energy has to be greater than or, at least, equal to the band gap energy (E_{BG}) of the material [57]. The band-gap is therefore the minimum energy required to move an electron from the valence band to the conduction band of a material at a particular temperature. In semiconductors, this energy decreases with temperature. A photon (E_{PH}) energized electron (negative) leaves behind a hole (positive) causing charges separation across the material. Figure 2.1 is an illustration of this phenomenon. Excess energy is converted into heat. Also, the freed electron may give up its absorbed energy in the form of heat and fall back to recombine with a hole in the valence band.

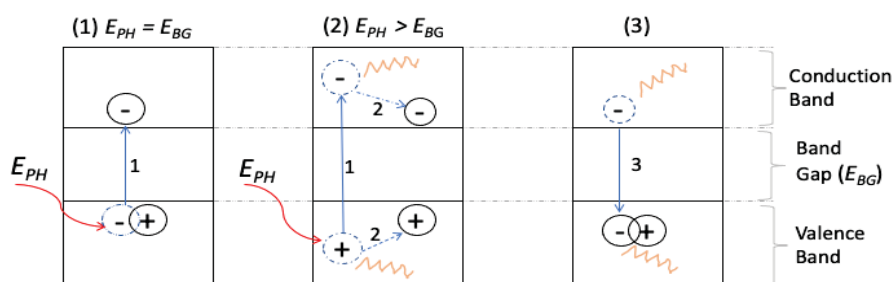


Figure 2.1: Photon absorption in a semi-conductor with band-gap E_{BG} showing the following scenarios: (1) E_{PH} excites an electron into the conduction band leaving behind an electron; (2) For $E_{PH} > E_{BG}$, the excess energy is converted to heat; (3) the excited electron gives up its energy as heat to recombine with a hole. [57]

A solar cell is commonly configured as a positive-negative (p-n) junction made from silicon resources. The positive-negative (p-n) junctions of silicon solar cells are made by diffusing an n-type dopant into one side of a p-type wafer (or vice versa). A simplified

structure of a solar cell showing silicon p-n junction is shown in Figure 3. When light of suitable wavelength is incident on the cell, it causes photovoltaic effect across the junction. Excess absorbed light energy is converted to heat.

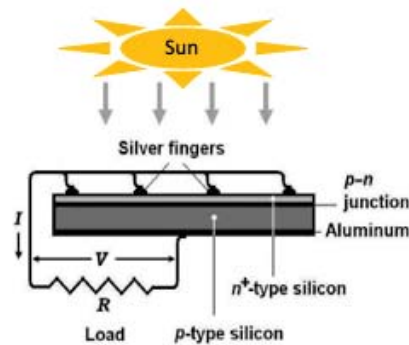


Figure 2.2: Structure of a solar cell showing silicon p-n junction and electrical contacts [58].

Solar cell technologies

Solar cell technology is an evolving one with ongoing research to improve both their performance and cost-effectiveness. This has led to many other solar cell technologies (See Table 2.1 for some examples). The traditional crystalline silicon cells are classified as first-generation cells. These cells may be monocrystalline or polycrystalline silicon with large grain sizes. Although they are more efficient at lower temperatures, they are also expensive to manufacture. They are however the most dominant type of PV cells in the market due to their stable power output over longer periods [59]. Thin-film cells are considered as the second-generation PV cells. They are cheaper than the first-generation cells because they require less silicon material. They however have a smaller share of the market because of their lower efficiency and precarious power output with time [59]. Some examples of thin-film technology cells include Amorphous silicon (a-Si), Cadmium telluride (CdTe) and Copper indium gallium selenide (CIGS). The third-generation cells include a range of alternative cells with the potential to overcome the Shockley-Queisser limit of 31-41% power efficiency for single bandgap solar cells [60]. Some common technologies for third generation cells are tandem cells (or multi-layer) cells, dye-sensitized cells, organic solar cells, perovskite solar cell and nano-crystalline (or quantum dot) solar cell [61]. Notwithstanding, some other indirect technologies - such as parabolic troughs, power towers, dish/engine systems and linear Fresnel reflectors - use concentration techniques to produce hot steam for electricity generation [62].

PV equivalent circuit.

An ideal solar cell behaves like a current source connected in parallel with a diode [63]. The current source generates electrical current, I_{ph} , when exposed to solar energy (photons). However, during darkness the solar cell behaves like a diode and generates current, called the diode or dark current (I_D), when connected to an external large voltage supply. This ideal model is completed with resistors to represent the losses and sometimes with additional diodes that take into account the current generated from the recombination of electrons and holes in the depletion region which dominates at lower forward-bias voltages. Figure 2.3 shows the most common solar cell equivalent circuit [63], comprising a current source, one diode and two resistors. The series resistor, R_S , takes into account losses in cell solder bonds, interconnection, junction boxes, etc., whereas the shunt resistor, R_{SH} , takes into account the current leakage (I_{SH}) through the high conductivity shunts across the p-n junction.

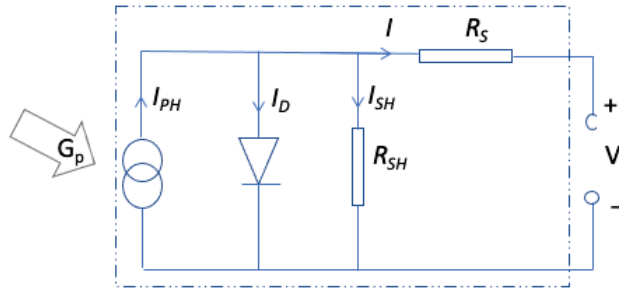


Figure 2.3: An equivalent solar cell circuit

From Kirchhoff's current law, the output current I produced by the solar cell is given as:

$$I = I_{ph} - I_D - I_{SH} \quad (2.1)$$

From the Shockley ideal diode equation or the diode law, I_D can be expressed as [60]:

$$I_D = I_o \left[\exp \left(\frac{V_D}{nV_T} \right) - 1 \right], \quad (2.2)$$

where I_o is the reverse bias (or dark) saturation current, V_D is the voltage across the diode, V_T is the thermal voltage, and n is the ideality factor ranging from 1(ideal) to 2. The dark saturation current (I_o) is an extremely important parameter that differentiates one diode from another [64]. I_o is a measure of the recombination of charge pairs in a device. A diode with a larger recombination will have a larger I_o . The thermal voltage can be expressed as:

$$V_T = \frac{kT}{q}, \quad (2.3)$$

where k is the Boltzmann constant (1.602×10^{-19} J/V), T is the absolute temperature of the p-n junction, and q is the electron charge (1.381×10^{-23} J/K). Thus, the characteristic equation, which relates the solar cell parameters to the output current and voltage can be expressed as [65]:

$$I = I_{ph} - I_0 \left[\exp\left(\frac{q(V+IR_S)}{nkT}\right) - 1 \right] - \frac{V+IR_S}{R_{SH}}, \quad (2.4)$$

Open circuit voltage

The main parameters that are used to characterize the performance of solar cells are the open circuit voltage V_{oc} , short circuit current I_{sc} , fill factor FF and the maximum power. The conversion efficiency (η) can be determined from these parameters. The extreme current-voltage situations of Equation (2.4) can be used to determine V_{oc} and I_{sc} .

The open-circuit voltage (V_{oc}) is the voltage at which no current flows (i.e., $I = 0$) through the external circuit. It is the maximum voltage that a solar cell can deliver. The V_{oc} corresponds to the forward bias voltage at which the dark current density compensates the photocurrent density. Thus, from Equation (2.4), for $I = 0$, $V_{oc} = V$, $R_{SH} \gg R_S$ and $I_{ph} \gg I_0$:

$$V_{oc} = \frac{kT}{q} \ln\left(\frac{I_{ph}}{I_0} - 1\right) \approx \frac{kT}{q} \ln\frac{I_{ph}}{I_0} \quad (2.5)$$

Short circuit current

The short circuit current, I_{sc} , is the current through the solar cell when the voltage across it is zero (i.e., $V = 0$). Thus, for short circuit condition, Equation (2.4) can be re-written as:

$$I_{sc} = I_{ph} - I_0 \left[\exp\left(\frac{qI_{sc}R_S}{nkT}\right) - 1 \right] - \frac{I_{sc}R_S}{R_{SH}}. \quad (2.6)$$

The value of each term in the expression has shown that the second term of the expression is comparatively insignificant [66]. As a result, the second term of the right side of Equation (2.6) can be neglected [65] and the expression can be rewritten as:

$$I_{sc} = \left(\frac{R_{SH}}{R_{SH}+R_S}\right) I_{PH}. \quad (2.7)$$

Equation (2.8) shows that for an ideal solar cell at minimum resistive losses (or ideal situation), the short-circuit current and the photo-generated current are identical. Therefore, I_{sc} is the largest current which may be drawn from the solar cell.

Thus, at $T = 25\text{ }^{\circ}\text{C}$, $n = 1$ and $R_{SH} \gg R_S$, the output current (Equation 2.4) and the open circuit voltage (Equation 2.5) can be approximated as:

$$I = I_{ph} - I_o[\exp(38.9V) - 1] \quad (2.8)$$

and

$$V_{oc} = 0.0257 \ln \frac{I_{ph}}{I_o} \quad (2.9)$$

From discussions so far, a plot of current-voltage (I-V) relation shows the extreme current and voltage conditions I_{sc} and V_{oc} respectively. The I-V curve of a PV module (or string) describes its energy conversion capability at the existing conditions of irradiance (light level) and temperature. A typical I-V curve of solar cells' single diode model is shown in Figure 2.4. It also shows the maximum power point (MPP), P_{MPP} . The solar cell should be operated at the maximum power voltage (V_{MPP}) to gain the MPP. The key electrical parameters highlighted in Figure 2.4 are generally provided by the manufacturer of the solar cell (or module).

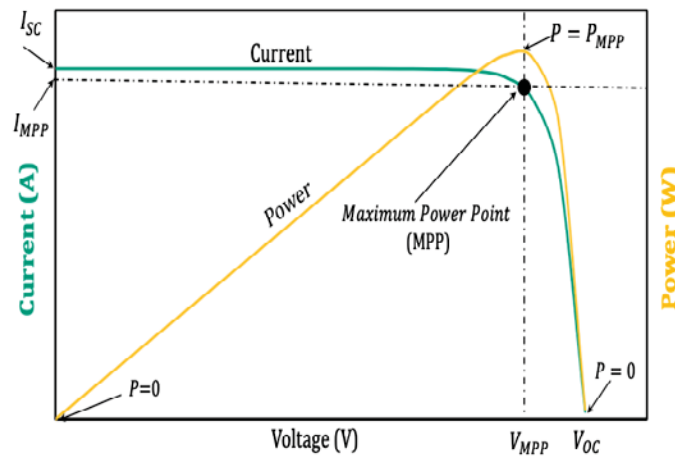


Figure 2.4: A typical I-V curve showing power profile

From the electrical power expression (i.e., $P = IV$), V_{MPP} occurs at the point where $dP/dV = 0$. Modern inverters in PV systems constantly adjust the load, seeking out the maximum operating power point at changing weather conditions.

Fill factor, FF

Although maximum current and voltage conditions for the solar cell are I_{SC} and V_{OC} respectively, Figure 2.4 shows that at both operating points, the power from the solar cell is zero. The fill factor, FF , is defined as the ratio of the maximum power from the solar cell to the product of V_{OC} and I_{SC} so that

$$FF = \frac{P_{MPP}}{V_{OC} \times I_{SC}} = \frac{V_{MPP} \times I_{MPP}}{V_{OC} \times I_{SC}} \quad (2.10)$$

The FF factor depends on the solar cell technologies which influence the shape of the IV curve. Table 2.1 shows V_{OC} , I_{SC} , FF and efficiencies of some selected technologies.

Effect of cell temperature on I-V curve

Environmental conditions, such as temperature or irradiation variations modify the I-V curve [67], and hence, influence the overall performance (energy yield) of solar cells. These variations affect the boundary conditions of the equations and, accordingly, the value of the equivalent circuit parameters. When temperature rises, whereas I_{SC} increases marginally, V_{OC} decreases significantly and the resultant P_{MPP} curve also decreases [63]. Figure 2.5 shows an example of variation of I-V curve of a silicon solar PV module with temperature. These variations are approximately linear with temperature, and most solar panel manufacturers include the rate of variation of the characteristic I-V curve points in the datasheets, either as absolute increase or as percent variation (please see Appendix E for an example of such data sheet). The variations with temperature on current and voltage levels variables, α , (e.g., V_{OC} , I_{SC} and P_{MPP}) can be expressed as [63]:

$$\vartheta_{T_c} = \vartheta_{T_{ref}} \left[1 + \frac{\epsilon_{\vartheta}}{100} (T_c - T_{ref}) \right], \quad (2.11)$$

where ϑ_{T_c} is parameter value at cell temperature T_c , $\vartheta_{T_{ref}}$ is parameter value at reference temperature T_{ref} and ϵ_{ϑ} is the temperature coefficient of ϑ expressed as a percentage change in the variable value with respect to a unit change in temperature ($\epsilon\%/^{\circ}\text{C}$). The temperature coefficient is dependent on the solar cell technology and may differ from one technology to another.

Table 2.1: Selected parameters of different cell technologies tested under the global air mass 1.5 spectrum (1000 W/m²) at 25°C [61]

Generation	Technology	Efficiency (%)	V _{oc} (V)	I _{sc} (mA/cm ²)	FF (%)	Test Centre (Date)	Description
First	Mono-crystalline silicon (mc-Si)	26.7 ± 0.5	0.738	42.65	84.9	AIIST *1 (3/17)	Kaneka n-type rear IBC
	Poly-crystalline silicon (pc-Si)	20.4 ± 0.3	0.665	66.36	77.2	FhG-ISE *2 (10/19)	Hanwha Q cells
Second	Amorphous silicon (a-Si)	10.2 ± 0.3	0.896	16.36	69.8	AIIST (7/14)	AIIST
	Cadmium telluride (CdTe)	21.0 ± 0.4	0.876	35.25	79.4	Newport (8/14)	First solar
Third	Copper indium gallium selenide (CIGS)	23.4 ± 0.5	0.734	39.58	80.4	AIIST (11/18)	Solar Frontier
	Organic thin film	18.2 ± 0.2	0.897	25.72	78.9	NREL*3 (10/20)	SJTU *4 Shanghai
	Dye sensitized	12.3 ± 0.4	1.02	15.17	79.1	Newport (8/19)	EPFL
	Nc-Si (nano crystalline) or quantum dots	11.9 ± 0.3	0.55	29.7	75.0	AIIST (2/17)	AIIST
	InGaP/GaAs/InGaAs	37.9 ± 1.2	3.065	14.27	86.7	AIIST (2/13)	Sharp, two-terminal
	Five-junction cell (bonded)	38.8 ± 1.2	4.76	9.56	85.2	NREL (7/13)	Spectrolab, two-terminal
	Perovskite/CIGS	24.2 ± 0.7	1.77	19.24	72.9	FhG-ISE (1/20)	HZB *5, two-terminal

*1 AIIST: Japanese National Institute of Advanced Industrial Science and Technology

*2 FhG-ISE: Fraunhofer Institut für Solare Energiesysteme

*3 NREL: National Renewable Energy Laboratory

*4 SJTU: Shanghai Jiao Tong University

*5 HZB: Helmholtz Zentrum Berli

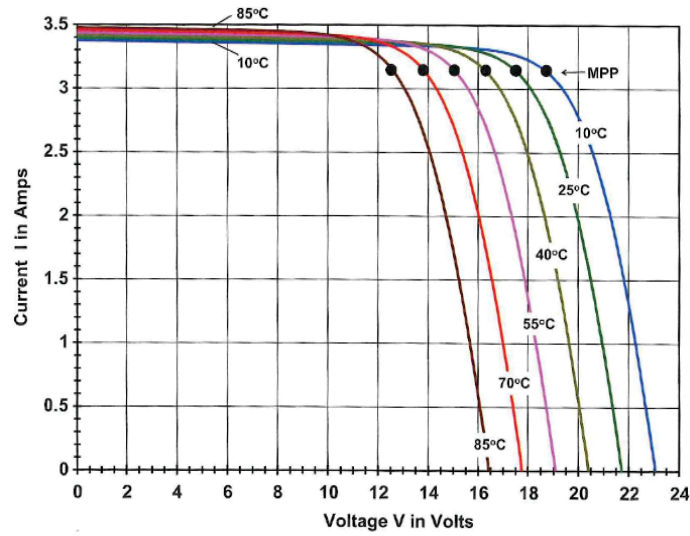


Figure 2.5: An example of variations in IV curves with temperature for a Siemens M55 monocrystalline solar module, at various cell temperatures and 1 kW/m² insolation [68].

Electrical Efficiency

Efficiency of energy systems are generally expressed as output over input energy. Nonetheless, the instantaneous electrical efficiency, η_{el} , of a crystalline solar cell could be expressed as a function of its temperature (T_c) [69]

$$\eta_{el} = \eta_0[1 - \beta(T_c - 25)], \quad (2.12)$$

where η_0 is the efficiency at standard test condition (STC) (Irradiance = 1000 W/m² and $T_c = 25$ °C), T_c is the solar cell temperature and β is the temperature dependent coefficient of electrical efficiency. As stated in the previous section, β differs with different PV materials used [about 0.0045/K for crystalline silicon, 0.0035/K for copper indium selenide (CIS), 0.0025/K for Cadmium telluride (CdTe) and 0.002/K for amorphous Silicon (a-Si)]. Efficiency of energy systems are generally expressed as output over input energy. Figures 2.5 and 2.6 show that the performance of the solar PV is directly affected by cell temperature.

The photovoltaic efficiency of solar cells is temperature dependent and it generally decreases with the increasing temperature (see Figure 2.6) due to the worse mobility of carriers, diffusion length, as well as lifetime of minority carriers and saturation current. Silicon photovoltaic cells are good absorbers, so their temperature rises significantly

during operation [67]. Thus, to improve the performance of the PV, the cells must be operated at controlled temperatures. One method for achieving that is by extracting the nuisance heat using a thermal absorber on the back of the PV to extract the heat. The most popular PVT technology is the flat plate PVT system.

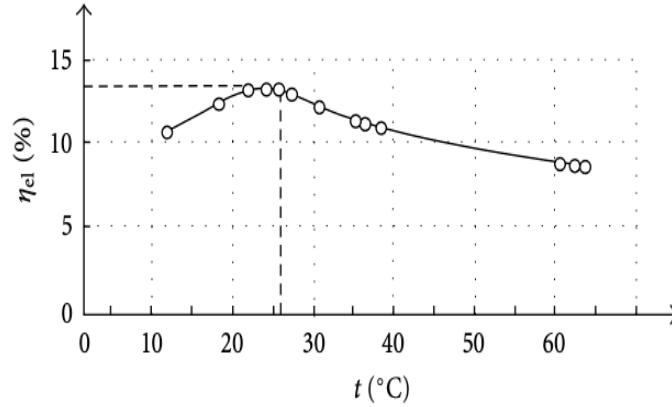


Figure 2.6: Efficiency of a crystalline silicon PV with $\eta_0 = 13.7\%$ as a function of cell temperature [67].

2.2 Fundamental theory of thermal energy transfer

Electromagnetic radiation interaction with surfaces

Heat energy can be transferred either by conduction, convection or radiation. Thermal radiation travels at the speed of light ($S \approx 300,000$ km/s in a vacuum) and is related to the wavelength (λ) and frequency (f) as:

$$S = \lambda f \quad (2.13)$$

When a beam of thermal radiation of wavelength, λ , is incident on a surface, a fraction of it is either reflected, absorbed and or transmitted in phenomena known respectively as reflectivity (ρ), absorptivity (α) and transmissivity (τ). These quantities are related as:

$$\rho + \alpha + \tau = 1 \quad (2.14)$$

A hypothetical blackbody absorbs all impinging thermal radiation such that $\rho = 0$, $\tau = 0$, and $\alpha = 1$. A blackbody is not just a perfect absorber but also characterized by emission of thermal radiation. Max Planck expressed the monochromatic emissive power (rate of energy emission per unit) of a blackbody in terms of temperature and wavelength as [70]

$$P_{b\lambda} = \frac{C_1/r_i^2}{\lambda^5(e^{C_2/\lambda T} - 1)}, \quad (2.15)$$

where $P_{b\lambda}$ is the monochromatic emissive power of a blackbody ($\text{W}/\text{m}^2 \mu\text{m}$), T is absolute temperature of the surface (K), $C_1 = 2\pi h S_0^2 = 3.74177 \times 10^8 \text{ W } \mu\text{m}^4/\text{m}^2$, $C_2 = hS_0/k =$

$1.43878 \times 10^4 \mu\text{m K}$, h is Plank's constant, S_o is speed of light in a vacuum, k is Boltzmann's constant and r_i is the refraction index of the medium.

The total emissive power, P_b , is related to $P_{b\lambda}$ as

$$P_b = \int_0^\infty P_{b\lambda} d\lambda = \sigma T^4 \quad (2.16)$$

Equation (2.16) is the Stefan-Boltzmann law of radiation [71], where σ is the Stefan-Boltzmann constant ($5.6697 \times 10^{-8} \text{ W/m K}^4$). Also, the ratio of the total emissive power, P_b , of a real surface to that of a blackbody, P_e , with both surfaces at the same temperature, is known as emissivity, ε , of the real surface expressed as:

$$\varepsilon = \frac{P_e}{P_b} \quad (2.17)$$

For a real surface, the rate of total radiant energy leaving a surface per unit surface area is called the radiosity (J). The radiant energy leaving the surface includes its original emission and any reflected rays given as [72]:

$$J = \varepsilon P_b + \rho G_T \quad (2.18)$$

where G_T is the irradiation incident on the surface per unit area.

Coefficient of thermal radiation

For two black surfaces separated by non-absorbing medium, the fraction of radiation leaving surface say A_1 that reached surface A_2 is defined as the view factor, F_{12} and is given as [72]

$$Q_{1 \rightarrow 2} = P_{b1} A_1 F_{12} \quad (2.19)$$

The reverse of $Q_{2 \rightarrow 1}$ is also true for (2.19). If both surfaces are emitting, while absorbing all incident radiation from the other surface at the same time, the net radiation exchange between the two black surfaces is given by [72]:

$$Q_{12} = A_1 F_{12} (P_{b1} - P_{b2}) = A_2 F_{21} (P_{b1} - P_{b2}) \quad (2.20)$$

$$(P_{b1} - P_{b2}) = \frac{1}{A_1 F_{12}} Q_{12} = \frac{1}{A_2 F_{21}} Q_{12} \quad (2.21)$$

In an electrical circuit analogy, the term $(P_{b1} - P_{b2})$ is an energy potential difference, Q_{12} represents the flow of the energy, whereas the terms $1/A_2F_{21}$ and $1/A_1F_{12}$ represent the resistances due to the geometric configuration of the two surfaces [70]. If we assumed surface temperatures of T_1 and T_2 for surface A_1 and A_2 respectively, Q_{12} can be written as:

$$Q_{12} = A_1F_{12}\sigma(T_1^4 - T_2^4) = A_2F_{21}\sigma(T_1^4 - T_2^4) \quad (2.22)$$

For the case of opaque gray surfaces; $\tau = 0$, $\varepsilon = \alpha$ and the reflectivity $\rho = 1 - \alpha = 1 - \varepsilon$. From (2.18),

$$J = \varepsilon P_b + (1 - \varepsilon)G_p \quad (2.23)$$

The net radiant energy Q for the gray surface of area A is the difference between incident radiation and radiosity:

$$Q = A(J - G_T) = \frac{A\varepsilon}{1-\varepsilon}(P_b - J) \quad (2.24)$$

Thus, if (2.34) is compared to an equivalent electric circuit, $(1 - \varepsilon)/A\varepsilon$ is the surface resistance due to the its imperfection as an emitter and absorber of radiation relative to a black surface. However, if we consider two parallel gray surfaces A_1 and A_2 the net radiation exchanges is given as:

$$Q_{12} = A_1F_{12}(J_1 - J_2) = A_2F_{21}(J_1 - J_2) \quad (2.25)$$

Thus, when two gray surfaces exchange radiation, apart from their individual surface resistances, there is also space resistance ($1/A_1F_{12} = 1/A_2F_{21}$) existing between them. Figure 2.7 shows an illustration of resistances between two radiation exchanging surfaces. The net rate of radiation exchange between the two surfaces is given by [72]:

$$Q_{12} = \frac{\sigma(T_1^4 - T_2^4)}{\left[\frac{(1-\varepsilon_1)}{A_1\varepsilon_1}\right] + \frac{1}{A_1F_{12}} + \left[\frac{(1-\varepsilon_2)}{A_2\varepsilon_2}\right]} \quad (2.26)$$

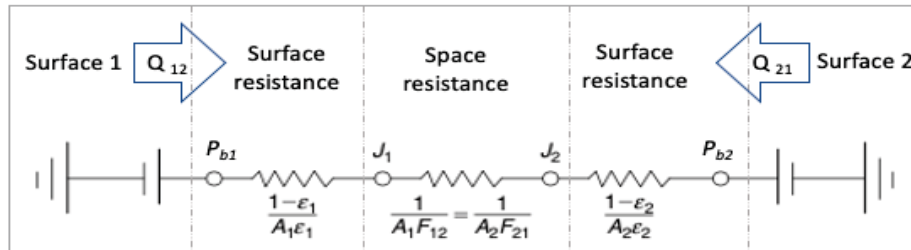


Figure 2.7: An illustration of radiation exchange between two gray surfaces showing equivalent electric network [72].

For two infinite parallel surfaces, $A_1 = A_2 = A$ and $F_{21} = 1$,

$$Q_{12} = \frac{A\sigma(T_1^4 - T_2^4)}{(1/\varepsilon_1) + (1/\varepsilon_2) - 1} \quad (2.27)$$

This can be written as:

$$Q_{12} = Ah_r(T_1 - T_2), \quad (2.28)$$

where

$$h_r = \frac{\sigma(T_1 + T_2)(T_1^2 + T_2^2)}{(1/\varepsilon_1) + (1/\varepsilon_2) - 1} \quad (2.29)$$

For a small convex surface, A_1 , completely enclosed by a very large concave surface, A_2 , $A_1 \ll A_2$ and $F_{12} = 1$:

$$Q_{12} = A_1 \varepsilon_1 \sigma (T_1^4 - T_2^4) \quad (2.30)$$

$$Q_{12} = A_1 h_r (T_1 - T_2), \quad (2.31)$$

where

$$h_r = \varepsilon_1 \sigma (T_1 + T_2)(T_1^2 + T_2^2) \quad (2.32)$$

The variable h_r is the radiation heat transfer coefficient for the different situations.

Coefficient of thermal convection

The convection heat transfer coefficient, h_c , is treated similarly in an equivalent circuit. Thus, if a wall at temperature T_2 is exposed to a cool fluid at temperature T_1 on one side, the convective heat-transfer rate can be given as [71]:

$$Q_c = Ah_c (T_2 - T_1) \quad (2.33)$$

Because of the many factors that affect the convection heat transfer coefficient, calculation of the coefficient is complex. The convective coefficient of heat transfer is calculated by Nusselt number (N_u), defined as the ratio of convection heat transfer to the fluid conduction heat transfer under same conditions. This can be expressed as [71]:

$$N_u = \frac{h_c L}{k_f} = Z R_e^a P_r^b \quad (2.34)$$

Where k_f is the thermal conductivity of the fluid in W/m K, L is representative dimension, R_e is Reynolds number given as $R_e = \dot{m}d/\omega$, P_r is Prandtl number given as $P_r = \omega c_p/k_f$, (Z , a , and b) are constant for the particular type of flow, \dot{m} mean mass flow rate, v is the

fluid flow rate, d characteristic linear dimension in m , ω is the dynamic viscosity in pascals and c_p is the specific heat capacity at constant pressure in $kJ/kg\ K$.

Thermal conduction

According to the second law of thermodynamics, heat will flow from the hot to the cold in an attempt to equalize the temperature difference, which is quantified in terms of heat flux Q . The heat flux is the rate per unit area at which heat flow in a given direction, which is directly proportional to the temperature difference δT and inversely proportional to the separation in distance δx .

$$\frac{dQ}{dt} = -k_c \frac{dT}{dx} \quad (2.35)$$

It could be seen from Figure 2.8 that the heat flow direction means temperature $T > T + \delta T$. The linear relation has a negative gradient, k_c , called the coefficient of thermal conductivity of the solid material.

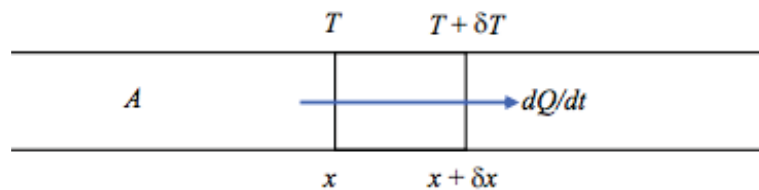


Figure 2.8: An illustration of heat flow through a conductor of cross section area A .

2.3 Fundamental theory of solar thermal collectors

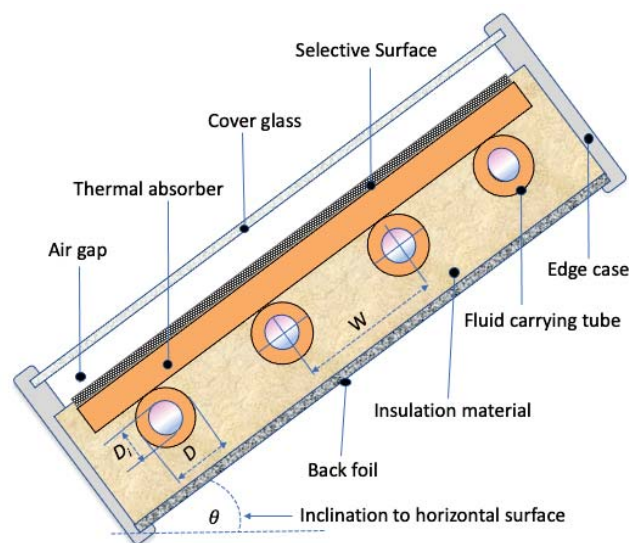


Figure 2.9: An illustration of a simple flat plate water thermal module

Solar thermal collectors convert solar energy directly into thermal energy. They are commonly designed as either flat-plate collectors, evacuated tube collectors, line focus collectors, or point focus/parabolic collectors. The flat-plate collectors may either be glazed (either single or multiple) or unglazed and may be coated with selective surfaces, such as tin oxide, and insulated to reduce losses. Some of the common fluid channel design in the absorber include parallel plates, header-riser, serpentine and bionic. The thermal energy transfer medium is predominantly by air, liquids or both. Figure 2.9 shows a simplified water based flat-plate solar collector.

Flat plate water thermal absorber and thermal losses

The general performance of the flat plate solar thermal collector can be evaluated based on the Hottel–Whillier equations [73]. The thermal efficiency of a conventional flat-plate solar collector is the ratio of the useful thermal energy (Q_u) to the overall incident solar radiation (G_p). The maximum ratio of energy reaching the thermal absorber will be the product of the cover glass absorptance (α_g) and transmittance (τ_g). This could be expressed mathematically as:

$$Input = G_p(\alpha\tau)_{gl} \quad (2.36)$$

The total thermal losses are approximated as being proportional to the temperature difference between the absorber plate surface temperature, T_p , and the ambient temperature, T_a and it is expressed as:

$$Losses = U_L(T_p - T_a) \quad (2.37)$$

where U_L is the overall losses coefficient.

The introduction of a fluid as the main heat extraction agent means that a heat removal factor, F_R , must be used to account for the fluid flow rate, collector-to-fluid interface, and inherent properties of the transfer fluid itself. Thus, for a thermal collector of area A_{th} , the useful heat energy, Q_u , can be expressed as [73] :

$$Q_u = A_{th}F_R[G_p(\alpha\tau)_g - U_L(T_i - T_a)], \quad (2.38)$$

Summarily, the Hottel and Whillier-Bliss model (2.38) incorporates a heat removal factor, F_R which compares Q_u to the theoretical energy gain if the entire collector was kept at inlet temperature [74]. Thus F_R can be expressed as a function of fluid parameters as:

$$F_R = \frac{\dot{m}c_p(T_o - T_i)}{A_{th}[G_P(\alpha\tau)_g - U_L(T_i - T_a)]}, \quad (2.39)$$

where T_o outlet temperatures, respectively. The heat removal efficiency factor can also be expressed as follows [73] [70]:

$$F_R = \frac{\dot{m}c_p}{A_{th}U_L} \left[1 - \exp\left(\frac{A_{th}U_L F_C}{\dot{m}c_p}\right) \right], \quad (2.40)$$

where F_C is the collector efficiency factor expressed as:

$$F_C = \frac{1/U_L}{W \left[\frac{1}{U_L[D+(W-D)F]} + \frac{1}{C_b} + \frac{1}{\pi h_{fi}D_i} \right]}, \quad (2.41)$$

where h_{fi} is the heat-transfer coefficient of the fluid, W is the pipe spacing, C_b is the conductance of the bond between the fin and copper circular pipes, D is the external diameter of the pipes, D_i is the internal diameter of the pipes and F is the fin efficiency factor expressed as [70]:

$$F = \sqrt{\frac{U_L}{k_{th}l_{th} + k_g l_g}}, \quad (2.42)$$

where l_{th} is the absorber thickness, k_{th} is the absorber thermal conductivity, l_g is the cover glass thickness and k_g is the cover glass thermal conductivity. If it is assumed that all losses occur to a common sink temperature T_a , then the overall loss coefficient (U_L) of the collector is the sum of the edge (U_e), top (U_t) and the back (U_b) loss coefficients, expressed as:

$$U_L = U_b + U_e + U_t \quad (2.43)$$

Assuming U_b is limited to heat flow through the back insulation material only, then it can be estimated as:

$$U_b = \frac{k_b}{l_b}, \quad (2.44)$$

where k_b is the insulation conductivity and l_b is the back insulation thickness. For most collectors the evaluation of edge losses is complicated. However, in a well-designed system, the edge loss should be small so that it is not necessary to predict it with great accuracy [70]. The edge losses could be estimated as:

$$U_e = \frac{k_b R l_{th}}{l_e A_{th}}, \quad (2.45)$$

where R is the collector perimeter, l_{th} is the collector thickness and L_e is the edge insulation thickness. Klein [75] has shown that the top losses can also be expressed as:

$$U_t = \left(\frac{N}{\frac{C}{T_p} \left[\frac{(T_{th} - T_a)}{(N+f)} \right]^e + \frac{1}{h_w}} \right)^{-1} + \frac{\sigma(T_{th} + T_a)(T_p^2 + T_a^2)}{\frac{1}{\varepsilon_{th} + 0.00591Nh_w} + \frac{2N+f-1+0.133\varepsilon_{th}}{\varepsilon_g} - N}, \quad (2.46)$$

where

N = number of glass covers

$f = (1 + 0.089h_w - 0.1166h_w\varepsilon_{th})(1 + 0.07866N)$

$C = 520(1 - 0.000051\theta^2)$

$e = 0.430(1 - 100/T_{abs})$

θ = collector tilt (deg)

ε_g = emittance of cover glass

ε_{th} = emittance of thermal absorber

h_w = wind heat transfer coefficient ($W/m^2 \text{ } ^\circ C$)

The thermal efficiency of the absorber, η_{th} , could then be determined from (15) as:

$$\eta_{th} = F_R(\alpha\tau)_g - U_L F_R \frac{(T_i - T_a)}{G_p}, \quad (2.47)$$

Equation (2.27) is a linear equation with η_{th} expressed as a function of $(T_i - T_a)/G_T$, ss could be seen from Figure 2.10.

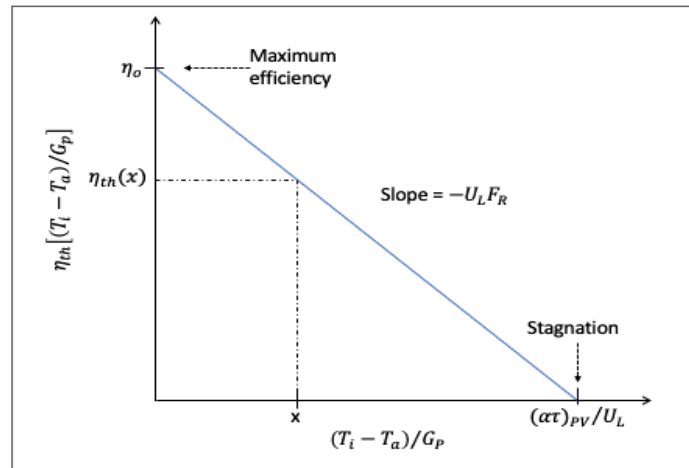


Figure 2.10: A plot of the thermal efficiency curve (2.47).

From Equation (2.38), when input energy becomes equal to energy losses, (i.e., $Q_u = 0$ and $\eta_{th} = 0$ (see Figure 2.10), equilibrium or stagnation temperatures is said to have

occurred. The equilibrium temperatures are substantially higher than ordinary operating temperatures. Once the plate temperature, T_p , can no longer increase, stagnation occurs. It can occur at higher radiation under no flow conditions, or on a cold, windy, clear day where convection and radiation losses are large and the heat loss coefficient, U_L , approaches the magnitude of the energy absorbed. The stagnation temperature could be estimated as:

$$T_p = T_a + \frac{(\alpha\tau)_{gl} G_P}{U_L}, \quad (2.48)$$

At these temperatures the pressure in the collector can be very high and most collector fluids either will have been boiled off or far exceeded their maximum working temperature [70]. Proper design of the collector fluid circuits can alleviate overheating problems. Figure 2.11 shows efficiency curves of some solar collectors and their suitable temperature applications.

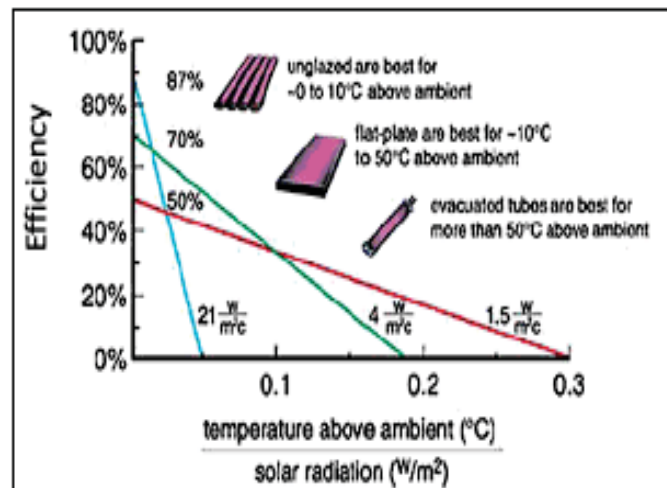


Figure 2.11: Efficiency curves of selected solar collectors showing operation temperatures and suitability [76].

2.4 Analytical model of energy in a PVT system.

The energy transition in the water based flat plate PVT module is summarized in Figure 2.12. This is based on the following assumptions: (1) Insulation in the back and the edges of the module are lossless, (2) There is no heat transfer in the direction of the flow, the energy transferred in the flow direction is by mass transfer, (3) Properties of glass and insulation are independent of temperature (constant), (4) All thermo-physical properties

of the fluid, air gap, and absorber are temperature, and (5) Dust and dirt on the collector are negligible.

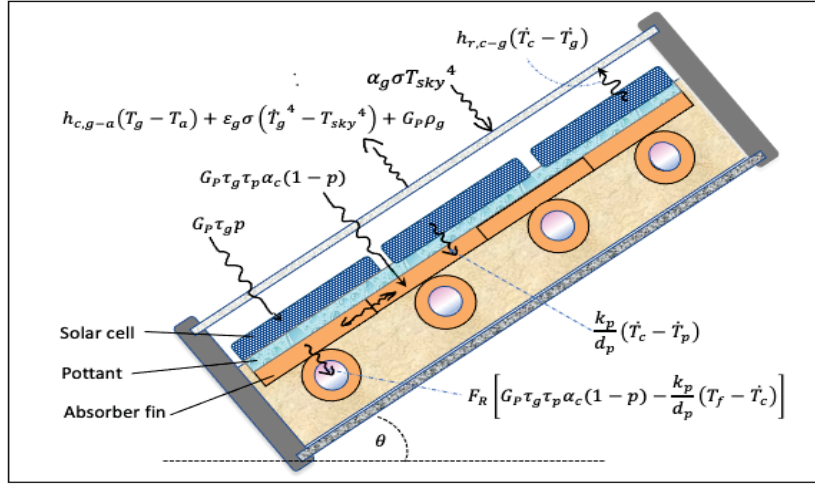


Figure 2.12: Energy transition in a water based flat plate PVT

The solar energy, per unit area, E_{g-c} , reaching the solar cell through the cover glass cover is given by

$$E_{g-c} = G_p \tau_g p \quad (2.49)$$

where τ_g is the transmittance of the glass cover and p is the parking factor of the cell envelope area. Assuming the cover glass is of very low iron content, it means absorption by the glass is negligible. Also, the absorptance of the solar cell, α_c , and τ_g are assumed to be close to unity and hence interreflection of insolation between the cells and the glass surface (s) is neglected. The electrical and thermal energy, per unit area, generated by the solar cell is given respectively as:

$$E_{c.el} = \eta_{el} G_p \tau_g p \quad (2.50)$$

where η_{el} is the cell electrical efficiency. Thus, thermal energy generated by the cell per unit area will be give as:

$$E_{c.th} = \alpha_c E_{g-c} - E_{c.el} - E_{c.l} \quad (2.51)$$

$$E_{c.th} = (\alpha_c - \eta_{el}) G_p \tau_g p - E_{c.l} \quad (2.52)$$

where $E_{c.l}$ is the solar cell energy losses, per unit area, which means that the thermal energy generated by the solar cell is partly lost to the top cover glass by a combination of natural convection and radiation. However, for a PVT, the airgap between the cell and the

cover glass is very thin and therefore losses by convection between cell and glass is assumed to be negligible. Thus $E_{c,l}$ is radiation dominated and is given as:

$$E_{c,l} = h_{r,c-g}(\dot{T}_c - \dot{T}_g) \quad (2.53)$$

where $h_{r,c-g}$ is the radiation heat transfer coefficient from cell to glass expressed as:

$$h_{r,c-g} = \frac{\sigma(\dot{T}_c + \dot{T}_g)(\dot{T}_c^2 + \dot{T}_g^2)}{(1/\varepsilon_c) + (1/\varepsilon_g) - 1} \quad (2.54)$$

where \dot{T}_c , \dot{T}_g , ε_c and ε_g are respectively the mean temperature for cell, mean temperature for glass, emissivity for cell and emissivity for glass. For energy conservation, $E_{c,l}$ is transmitted as part of energy losses by the cover glass to ambient. This is expressed as

$$E_{g,l-a} = h_{c,g-a}(T_g - T_a) + \varepsilon_g \sigma (\dot{T}_g^4 - T_{sky}^4) + G_P \rho_g \quad (2.55)$$

where $E_{g,l-a}$ is net energy per unit area from the glass to ambient, T_{sky} is sky temperature, ρ_g is reflectivity of the glass and $h_{c,g-a}$ is the convective heat transfer coefficient from glass to ambient. Stulz and Wen [77] have shown that

$$h_{c,g-a} = 1.247[(\dot{T}_g - \dot{T}_a) \cos \theta]^{1/3} + 2.658w \quad (2.56)$$

where θ is PVT module's inclination to the horizontal, \dot{T}_a mean ambient temperature and w is wind speed in m/s. Thus, the available thermal energy from the cell per unit area, that is not lost, which is transferred to the thermal plate is given as:

$$E_{c,th} = (\alpha_c - \eta_{el})G_P \tau_g p - h_{r,c-g}(\dot{T}_c - \dot{T}_g) \quad (2.57)$$

If we assume that the pottant between the cell and the thermal plate is infrared radiation opaque, then $E_{c,th-p}$ transfer of energy per unit area from the cell to the thermal plate will be only by conduction. Thus,

$$E_{c,th-p} = \frac{k_p}{d_p}(\dot{T}_c - \dot{T}_p) \quad (2.58)$$

where \dot{T}_p is the average plate temperature, k_p is the thermal conductivity of the pottant and d_p is the thickness of the pottant. This means that \dot{T}_p can be calculated from

$$(\alpha_c - \eta_{el})G_P \tau_g p - h_{r,c-g}(\dot{T}_c - \dot{T}_g) = \frac{k_p}{d_p}(\dot{T}_c - \dot{T}_p) \quad (2.59)$$

Aside $E_{c.th-p}$ there is also energy per unit area, E_{g-p} , due to insolation incident between the cells which is transmitted through the pottant to the thermal absorber which is given as:

$$E_{g-p} = G_p \tau_g \tau_p \alpha_c (1 - p) \quad (2.60)$$

We can now consider heat transfer to fins and subsequently to the tubes along the flow length. From Hottel and Whillier [73], the heat transfer by tubes to the fluid at temperature T_f is given by:

$$Q_{th} = A_{th} F_R \left[G_p \tau_g \tau_p \alpha_c (1 - p) - \frac{k_p}{d_p} (T_f - \dot{T}_c) \right] \quad (2.61)$$

The losses coefficient in (2.61) - i.e. $U_L = k_p/d_p$ - shows that the absorber losses is only limited to the pottant (i.e. $U_e = U_b = 0$). Thus, F_R for the PVT can be expressed as:

$$F_R = \frac{\dot{m} C_p d_p}{A_{th} k_p} \left[1 - \exp \left(\frac{A_{th} k_p F_c}{\dot{m} C_p d_p} \right) \right], \quad (2.62)$$

where F_c is the collector efficiency factor expressed as:

$$F_c = \frac{d_p/k_p}{W \left[\frac{d_p}{k_p [D + (W-D)F]} + \frac{1}{C_b} + \frac{1}{\pi h_{fi} D_i} \right]}, \quad (2.63)$$

where h_{fi} is the heat-transfer coefficient of the fluid. F is expressed as:

$$F = \sqrt{\frac{k_p/d_p}{k_{th} l_{th} + k_p l_p}}, \quad (2.64)$$

Thus, the thermal efficiency η_{th} of the absorber could be determined from (60).

$$\eta_{th} = F_R \tau_g \tau_p \alpha_c (1 - p) - \frac{k_p}{d_p} F_R \frac{(T_f - \dot{T}_c)}{G_p}, \quad (2.65)$$

3 Materials and Methods

The methodology used in accomplishing the set objectives for this thesis includes design of experiment, installation of experimental set-up, data measurement and logging over the period of study, analyzing the data with relevant statistical tools. Figure 3.1 conceptualizes the logical relationships between the goal of the thesis, specific objectives, research edge as well as the approach research method. It also clearly shows how the individual research papers contribute to the overall thesis goal.

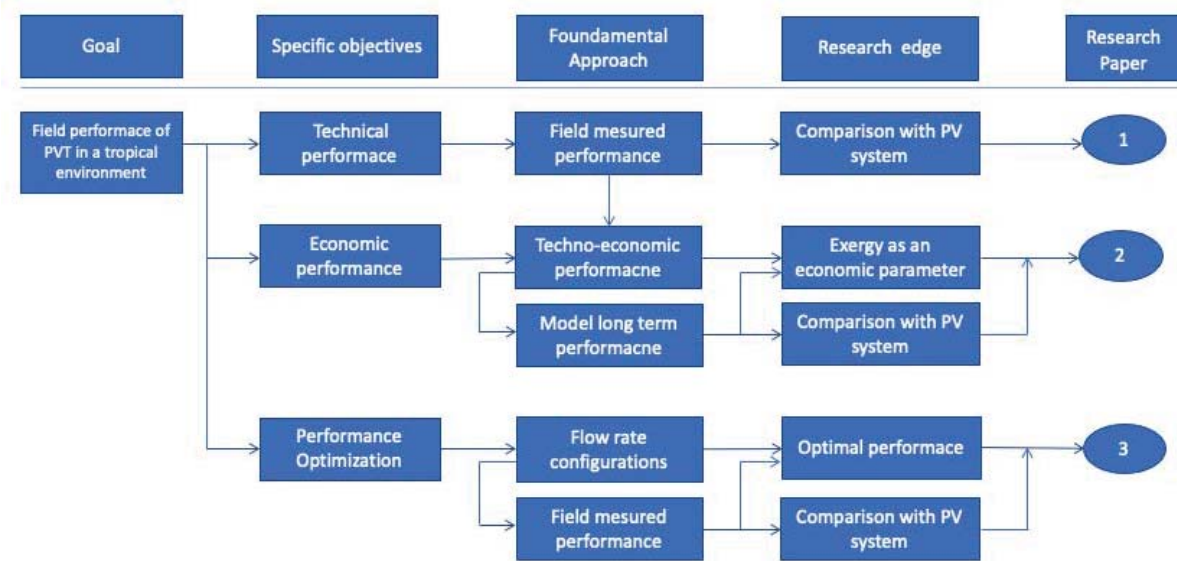


Figure 3.1: Conceptual Framework

3.1 Experimental design and set-up

Experimental design is a method used to organize, conduct, and interpret results of experiments in an efficient way, to obtain useful information through a small number of trials [78]. Proper organization of experiments is a foundation of every thoughtful research. The main goal of any experimental study is to find the relationships between independent variables (factors) and dependent variables (results, outcomes) within the experimental framework. Even though it sounds easy to accomplish, this task can be cumbersome when it is not organized correctly. Inevitably, decisions on an experimental design involve making difficult choices among options because of resource constraints while focusing on the main aim [78].

The experimental set-up for this thesis consists of conventional solar PV installation and hybrid PVT installation, as well as instrumental set-up for measuring ambient weather conditions and other variables. Figure 3.2 shows an elaborate schematic diagram of the experimental setup for this study as could be seen in Papers 1 and 3.

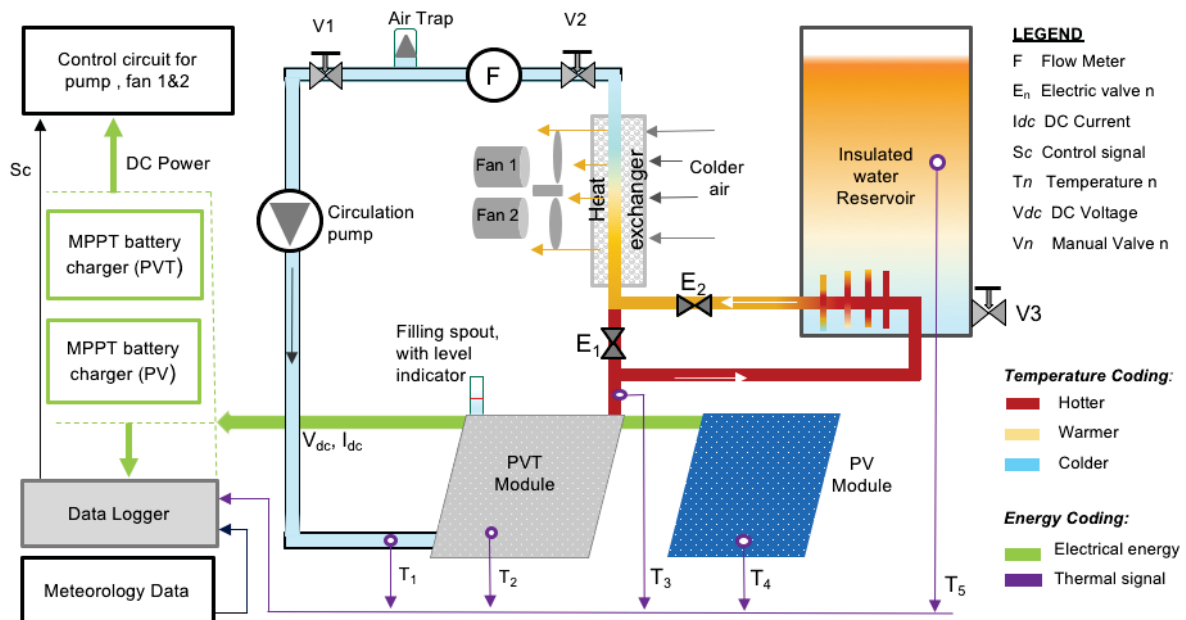


Figure 3.2: The schematic shows the interconnection of components, data measurement points and energy flow of the experimental setup.

The main heat transfer medium (fluid) for the PVT in the setup in Figure 3.2 has been by force-circulation of water. For a closed loop system, the absorber heat transfer fluid is important to the life, design, and operation of the system. Some popular transfer fluids include water, water/glycol mix, synthetic hydrocarbons and silicon. Given the location of the setup with no threats of freezing due to ambient conditions, water has been used in the collector loop because it is readily available, and, it has superior specific heat capacity to any other transfer fluid and it is economically cheaper to access. Water is also odorless and non-toxic in its pure state and therefore easier to handle. Water is also thermally stable and does not degrade with temperature. It therefore requires the use of simple single-walled heat exchangers with little dangers of contamination.

To transfer the thermal energy from the working fluid to the storage tank fluid requires a heat exchanger. The heat exchanger for the setup was made from a 3.6 m length of smooth surfaced cylindrical copper pipe with average external diameter of 0.015 m and

sheet thickness of 0.001 m. Copper pipe has been used because of its good heat conduction property. The copper pipe was coiled into 7 turns with a mean external coil diameter of 0.16 m and a mean pitch of 0.02 m. Figure 3.3 shows a picture of the heat exchanger. The heat exchanger has been placed inside the storage tank closer to its bottom. Heat transfer to stored water has been purely by convection due to gravity. Although the unconventional rule of thumb for sizing is approximately 0.2 m² heat exchanger surface per m² area of flat-plate collectors, this has not been strictly applied in this case because for hybrid collectors the generation of electric power could have a major influence on the thermal performance [72].

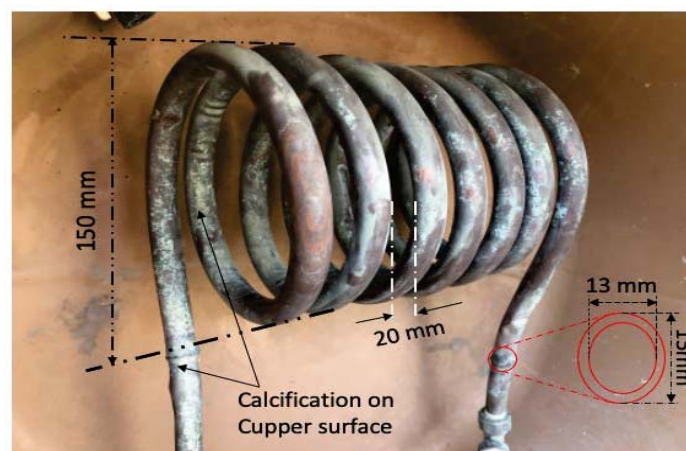


Figure 3.3: Heat exchanger with some dimensions

The main focus of the setup is on the performance of the modules, which is directly related to the fluid inlet temperature for the thermal absorber in the case of the PVT. Lower inlet temperature leads to higher collector efficiency [72] and also lower temperatures for PV cells. Thus, to further reduce the temperature of the returning working water, apart from the conventional heat exchanger in the storage tank, a radiator system has been included in the absorber loop. The radiator is made up of water-to-air heat exchanger with a pair of fans. The sizing of the radiator system was not based on any technical specifications. However, some design details could be found in Appendix F. The radiator system contributes to the performance of the setup in two ways: (1) An important aspect of thermal absorber testing is to keep the specific heat capacity (c_p) and density (ρ) of the fluid used within $\pm 1\%$ over the range of fluid temperatures used during the tests [79]. As could be seen from Figure 3.4, maintaining the inlet temperature between 25-40 °C ensures that ρ and c_p remain with $\pm 1\%$. Thus, radiator system reduces

the chaotic changes in the water inlet temperature - for a test facility in an erratic outdoor environment- and the influence of relatively higher storage water temperatures on the temperature of the returning inlet water. (2) Also, lowering the water inlet temperature relative to ambience reduces thermal losses (see Equation 2.47) and hence improves the efficiency of the setup.

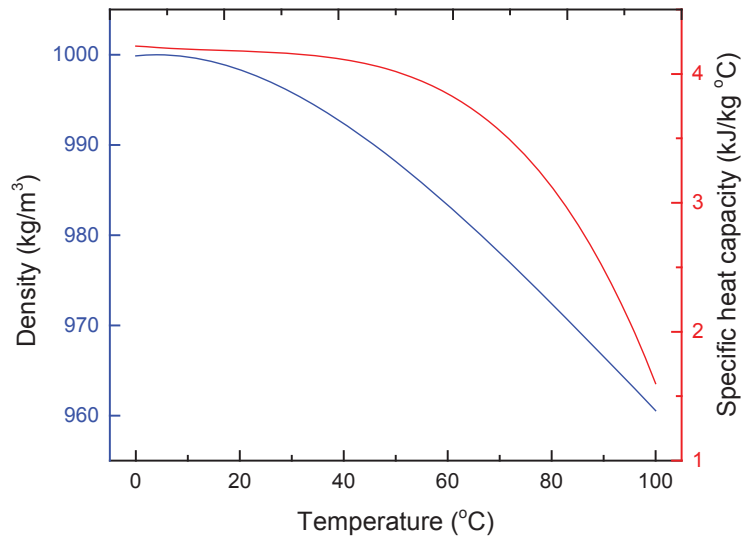


Figure 3.4: A variation of density and specific heat capacity of water with change in temperature at constant pressure of 1bar.

For normal operation of solar collectors, thermal capacitance is provided to alleviate the solar availability and load mismatch and improve the system response to sudden peak loads or loss of solar input. As stated earlier, this also improves the system's efficiency by preventing the heat transfer fluid from quickly reaching high temperatures, which lower the collector efficiency. The water storage tank for the setup is non-pressurized with the heat exchanger installed closer to its base. Figure 3.5 shows some details of the storage tank. The tank used for the study is a cylindrically-shaped 75L plastic thermos vessel with a very tight lid, originally for storing cold and hot substances over short periods for domestic use. This has always been filled to 70L for the study for consistency. The sizing was based on the typically rule of thumb of about 40–80 L per square meter of collector area [72]. To improve its insulation property, an additional 19 mm thick Armaflex sheet has been used to cover its outer curved surface and base. This was then finally covered with a thermal resistance foil to reduce its thermal interaction with the environment (see Appendix G for details). The lid was however not modified. The tank has also been fitted with a manual valve closer to the base to allow for easier emptying of content.



Figure 3.5: Some details of thermal storage vessel showing: (a) the thermos vessel, (b) armafex insulation, (c) heat exchanger, (d) spout for transducer insertion, (e) non modified lid, (f) thermal resistant foil cover and (g) manual valve

3.1.1 Working principle of the experimental setup

The basic principles of experimental designs are randomization, replication and local control. These principles make a valid test of significance possible. A good experimental setup should obtain relevant information with minimal risk of errors using as minimum resources as possible. As described in Papers 1-3, the operation of a water PVT system involves the working together of many sub-components to achieve desired results. Figure 3.8 shows a flow diagram of sequence of operation of the setup shown in Figure 3.2. As could be seen, the operating conditions depend on whether (irradiance in this case), selected mode of operation (1 or 2) and set variable limits. These are achieved by systematic control circuit with monitoring system (data logger in this case) and well balance load distribution of components to achieve maximum power point (MPPT) operation.

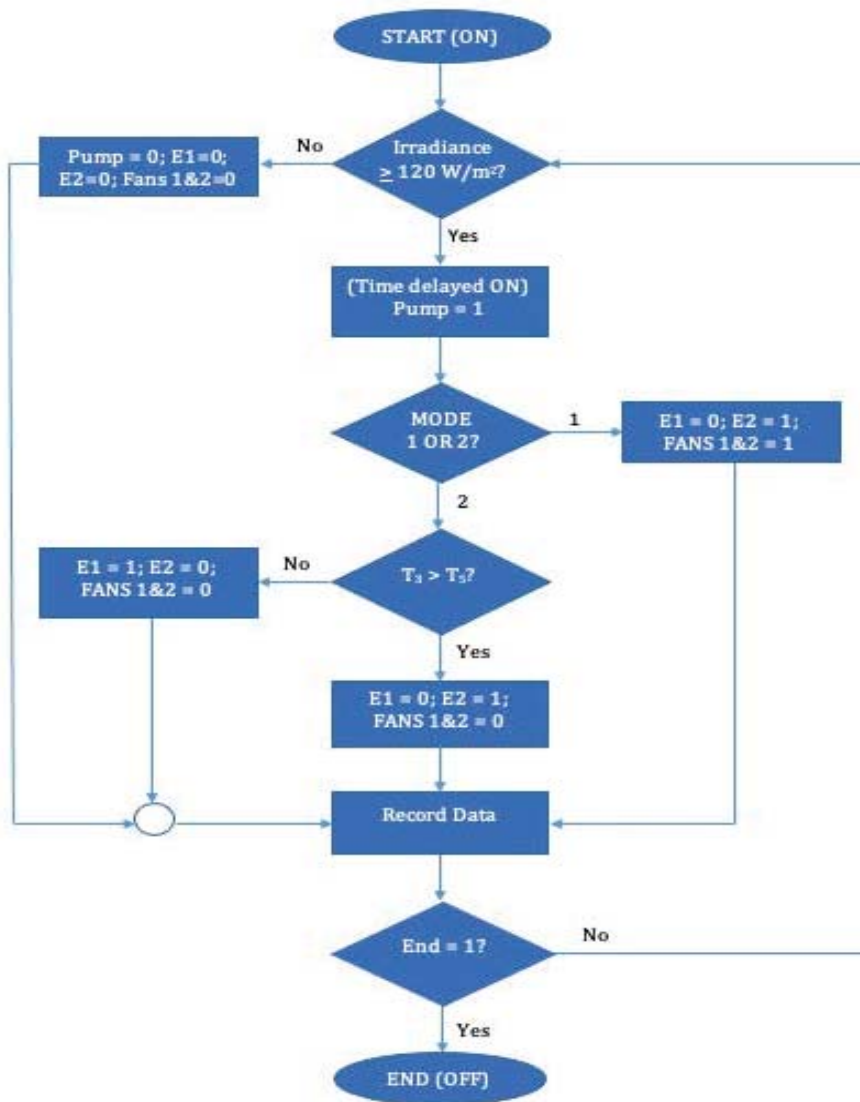


Figure 3.6: Flow diagram of working principle of the experimental setup

3.1.2 Control circuit

One method of reducing human errors in an experimental setup is to automate most of the repetitive activities. This is achieved by using intelligent control systems. As could be seen, Figure 3.7 illustrates a rough design of electrical loads distribution; showing battery chargers, batteries, pump, fans, data logger and the control circuit. This also means that the electrical energy required by the components in the setup is completely generated by the PV and PVT modules, making it an energy independent system. Figure 3.8 also shows fine details of how individual components are interconnected to create an intelligent control circuit (CCT) (Also see Appendices B and C). The CCT includes relays, switches and monitoring system (data logger). It could be seen from the CCT that the setup works

as a stand-alone unit with minimal human interventions. Also, both Figures 3.7 and 3.8 show fuses (i.e., F1-F8) in the circuits for protection against faulty components.

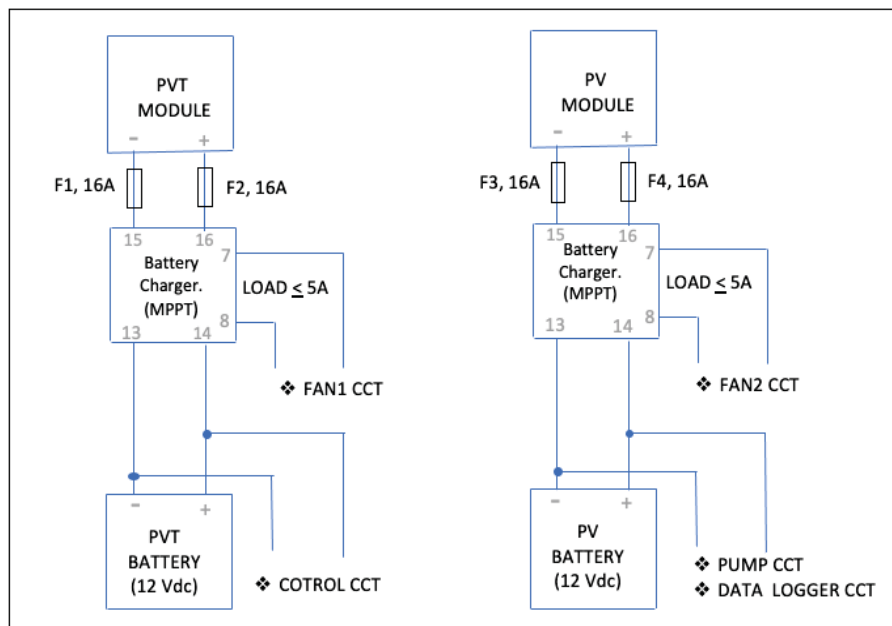


Figure 3.7: Electrical load distribution for PV and PVT sub-systems

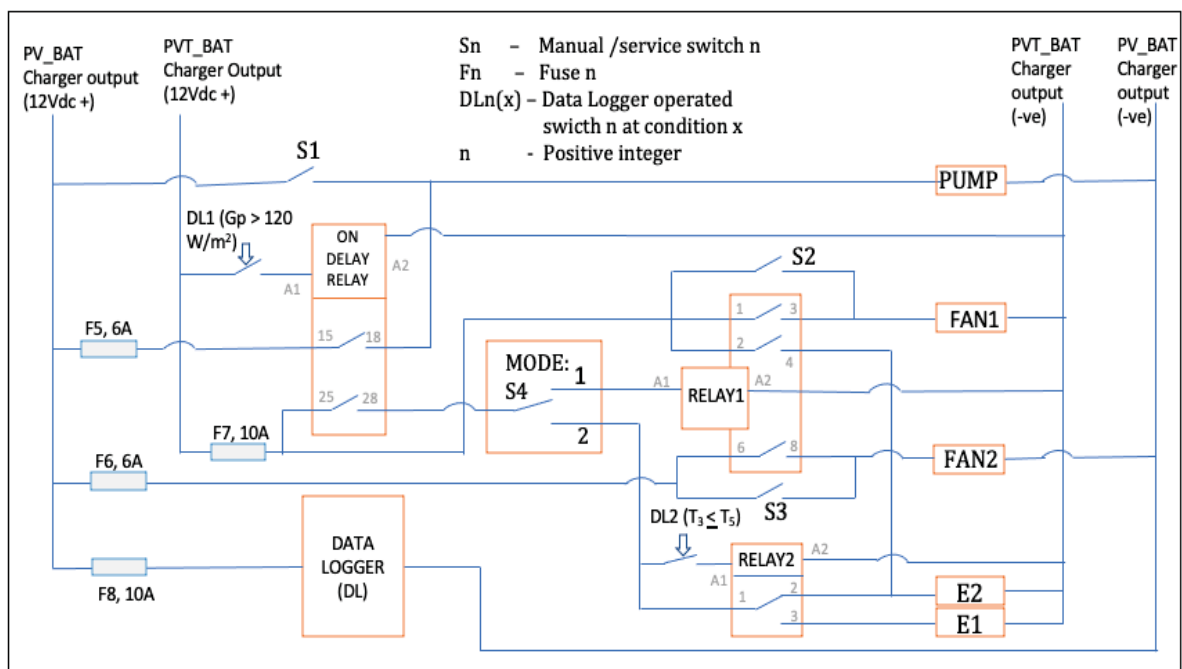


Figure 3.8: Control circuit showing detailed electrical load distribution and interconnections between control relays, switches, fuses and energy sources.

3.1.3 Modes of operation of the PVT sub-system

The PVT sub-system has been designed to operate in two fundamental modes. Figure 3.9(A) shows simplified line diagram of the PVT's closed-loop water circulation circuit in an idle state (pump off). As could be seen from Figure 3.6, this state of operation will occur in any of the modes when G_p (i.e., in-plane irradiance) $< 120 \text{ W/m}^2$.

Operation Mode 1 configuration is biased towards maximizing electrical energy output from the PVT module by cognizant cooling of circulating water in the closed-loop, resulting in relatively lower average cells temperature and hence subsequent improvement in electrical efficiency. In this mode, for experimental reasons, heat transfer to water in reservoir is compromised. Figure 3.9 (B) shows Mode 1 configuration. For an initial condition of $G_p \geq 120 \text{ W/m}^2$, the water is continuously circulated through the water reservoir and water-to-air heat exchanger and returns to the inlet of the PVT module relatively colder. This mode also reduces variations in T_1 to the barest minimum for the outdoor experimental setup. This configuration was used for collecting the primary data for Paper 1.

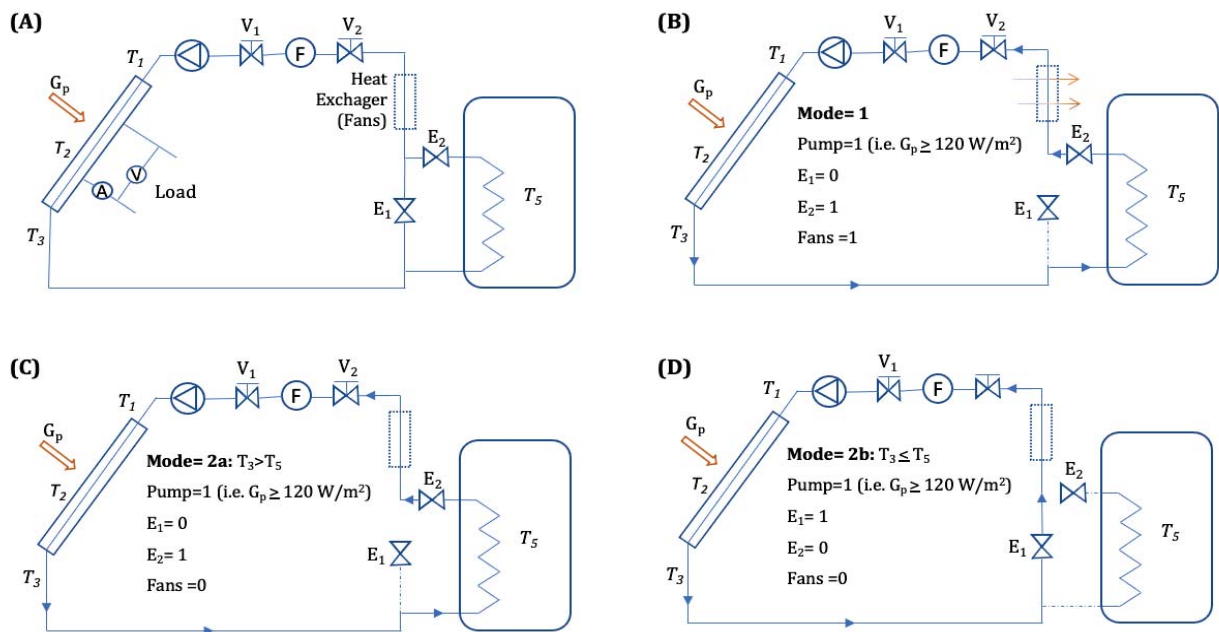


Figure 3.9: (A) Simplified line diagram of the PVT's closed-loop water circulation circuit in an idle state; (B) operational Mode 1 configuration; (C) operational mode 2 configuration when $T_3 > T_5$; (D) operational mode 2 configuration when $T_3 \leq T_5$

Operation Mode 2 explores the heating of stored liquid in a reservoir, a fundamental principle in domestic solar hot water systems. For initial conditions of $G_p \geq 120 \text{ W/m}^2$ and

$T_3 > T_5$, the warmer water from T_3 is continuously circulated through heat exchanger coil in the reservoir till any of the pre-conditions is breached. This configuration is illustrated in Figure 3.9(C). However, as could be seen from Mode 2b configuration shown in Figure 3.9(D), for $G_p \geq 120 \text{ W/m}^2$ and $T_3 \leq T_5$, the exiting water from T_3 is re-circulated through the PVT module until $T_3 > T_5$ when it reverts to configuration Mode 2a. These 2 modes (1 and 2) can be operated together to experiment different scenarios. Both configuration modes 1 and 2 were used in Papers 2 and 3.

3.1.4 Photovoltaic-thermal and Photovoltaic set-up

The experimental set-up for the PVT and PV used in this study was installed on the roof of the Department of Mechanical Engineering laboratory, Kwame Nkrumah University of Science and Technology (KNUST) Kumasi Ghana. The latitude and longitude of the installation are respectively 6.68°N and 1.57°W . Some pictures of the installations are shown in Figure 3.10. The PVT (model: Volther PowerVolt) and PV (model: PV SOL60S-270W) were manufactured and supplied by Solimpeks in Turkey [80]. Table 3.1 also shows some selected information for PV and PVT modules (Also, see Appendix E for technical details).



Figure 3.10: Installation of setup on the roof top of Solar Energy Applications Laboratory at Department of Mechanical Engineering, KNUST Ghana, showing; (A) PV and PVT modules; (B) North facing surface with water circulation and Electric/Data compartments; (C) East facing surface with radiator cooling fans

Table 3.1: Technical specification of PVT and PV collectors.

Parameters	PVT	PV
Manufacturer	Solimpeks, Turkey	Solimpeks, Turkey
Model	Volther PowerVolt	PV SOL60S-270W
Photocell type	mc-Si	mc-Si
Number of cells	72	72
Absorber surface (Thermal)	Copper	-
Module Dimension (mm ³)	1601x828x90	1640x992x45
Aperture Area A_m (m ²)	1.326	1.474
Absorber Area (m ²)	1.194	-
Weight (kg)	24.4	18.3
Nominal electrical power P_{max} (W)	200	270
Thermal Power (W)	630	-
Nominal current I_{mp} (A)	5.43	8.6
Short circuit current I_{sc} (A)	5.67	9.31
Nominal voltage V_{mp} (V)	36.8	31.4
Open circuit voltage V_{oc} (V)	46.43	38.3
Module electrical efficiency (%)	15.08	16.6
Zero loss collector efficiency (%)	47.5	-
Temperature Coefficient of I_{sc} (%/°C)	0.06	0.05
Temperature Coefficient of V_{oc} (%/°C)	-0.34	-0.34
Temperature Coefficient of P_{max} (%/°C)	-0.45	-0.45
Nominal operating cell temperature $NOCT$ (°C)	45±2	45±2

3.1.5 Instrumentations and data collection

A programable Campbell CR300 data logger has been used to record both meteorological and modules' performance data. The measurements are sampled every 10 seconds and then averaged over 15-minute periods, from which hourly, daily, and monthly data are determined. Table 3.2 shows the list of characteristics of the instrumentation used in this study (see Appendix D). Detailed description of instrumentations and data collection can be found in Papers 1 and 3.

Table 3.2: Test Variables and Sensors

Variable	Instrumentation	Measurement accuracy	Resolution
Temperature (°C)	109 Temperature Probe (Pt100)	±0.2 °C (for 0 to 70 °C)	0.01
Irradiance(W/m ²)	Apogee SP-421 pyranometer	±1%	<0.001
Wind speed (m/s)	Decagon DL-2 wind sensor	3%	0.01
Air temperature (°C)	CS215 Temp/RH sensor	±0.4 °C (5 to 40 °C)	0.01
Relative humidity (%)	CS215 Temp/RH sensor	±4% (0 to 100 %) at 25 °C	0.03
Flowrate (L/min)	Mechanical valves set.	Not specified	0.2
Current (A)	Bim205 smart charger w/MPPT	Not specified	0.1
Voltage (V)	Bim205 smart charger w/MPPT	Not specified	0.1

3.2 Climatic conditions at the installation site

The performance of a solar collector is influenced by many interactive weather factors and collector's related parameters. There is however, a very high level of variability and uncertainty in predicting meteorological variables. Nonetheless, PV cell temperature, for instance, is a function of ambient temperature, wind speed and global irradiance [27]. Ghana is a sub-Saharan African country with land mass located within latitude 5 °N - 11 °N and longitude 3 °W - 1 °E [81]. The installation site is in Kumasi, a town in the middle belt rain forest region of Ghana characterized by tropical rainfalls. By the Köppen-Geiger classifications, Kumasi's climate is classified as tropical savanna climate or tropical wet and dry climate of categories *Aw* (for a dry winter) and *As* (for a dry summer). This implies that the average temperature of the coolest month is above 18 °C and precipitation in the driest month is less than 60 mm [82].

In general, Ghana experiences two main climatic seasons namely, the wet and dry seasons. Typically, the wet season in Kumasi starts from April to October. It is normally characterized by cloudy weather conditions, relatively higher mean monthly precipitation, relatively lower mean ambient temperatures, and relatively lower average daily irradiance. The dry season (which predominantly spans November to March) records low-to-no precipitation, higher ambient temperatures, and higher irradiance.

The yearly average daily global insolation and the yearly average daily ambient temperature recorded at the installation site for the year 2019 were 4.05 kWh/m²/day and 27.13 °C respectively, as detailed in Figure 3.11 [83]. However, as could be seen from Figure 3.12, the monthly average wind speed is less than 1.00 m/s, which prospectively indicates that wind speed effects on solar photovoltaic performance could be negligible. However, occasional wind gusts ranging from 3 m/s in February to 11 m/s in October were observed during the period and must be considered in the design of mounting racks for the site.

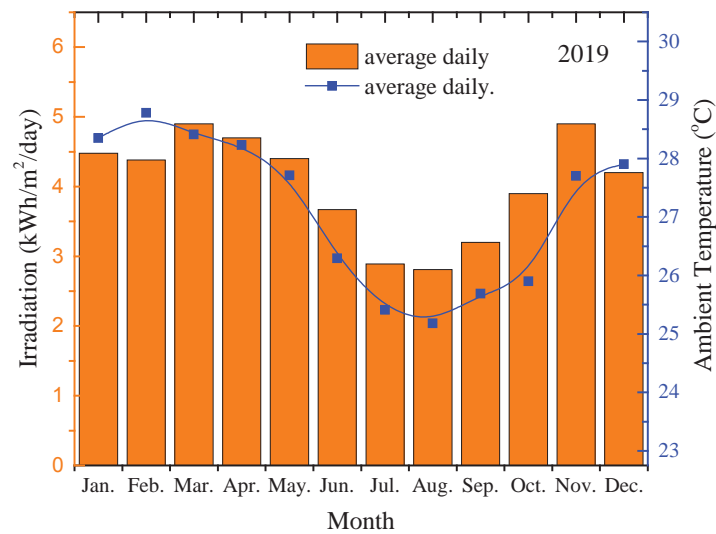


Figure 3.11: Monthly average daily irradiation and monthly average daily ambient temperature at the installation site for the year 2019

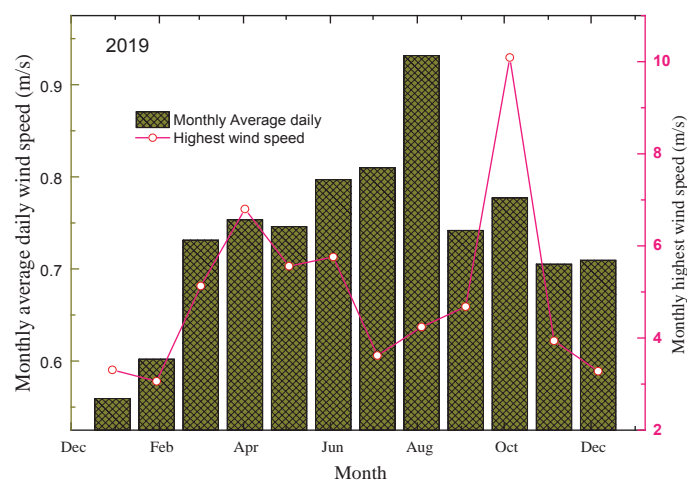


Figure 3.12: Monthly average daily wind speeds at the experimental site

3.3 Data analysis

3.3.1 Energy efficiency and analysis

The overall performance of a convectional PV system is usually examined using selected performance indices, which include energy yield, performance ratio and efficiency. In the case of hybrid PVT system, the overall performance is a combination of both convectional PV (electricity) indices and solar thermal (heat energy) system. The instantaneous electrical efficiency of a crystalline solar cell could be expressed as a function of its temperature (T_c) [69] as:

$$\eta_{el} = \eta_0[1 + \beta(T_c - 25)], \quad (3.1)$$

where η_0 is the efficiency at standard test conditions (STC) (which are defined as Irradiance = 1000 W/m², $T_c = 25$ °C, and air-mass ratio = 1.5), T_c is the solar cell temperature (i.e., T_2 and T_4 for PVT and PV respectively, from Figures 3.2 and 3.9) and β is the temperature dependent coefficient of electrical efficiency. The value of β differs with different PV materials used (about -0.0045/K for crystalline silicon, -0.0035/K for CIS, 0.0025/K for CdTe and -0.002/K for amorphous-Si).

Efficiency of energy systems are generally expressed as ratio of output energy to input energy. The PV module (cell) electrical efficiency (η_{el}) is, therefore, given as:

$$\eta_{el} = \frac{E_{dc}}{A_m * G_p}, \quad (3.2)$$

where E_{dc} is the direct current (DC) power from the module in kW, A_m is the module total surface area (m²) and G_p is the in-plane irradiance (kW/m²). Similarly, the thermal efficiency (η_{th}) is, also, expressed as:

$$\eta_{th} = \frac{E_{th}}{A_m \times G_p}, \quad (3.3)$$

where E_{th} is the useful thermal gains of the system and it is given as:

$$E_{th} = m_w c_p (T_o - T_i), \quad (3.4)$$

where m_w is the water mass flowrate (kg/s), c_p is the specific heat capacity of water (kJ/kg °C) and, T_i and T_o (i.e., T_1 and T_3 respectively, from Figures 3.2 and 3.9) are the inlet and outlet water temperatures respectively, in °C. The total efficiency of the integrated PVT (η_{PVT}) is used to evaluate the overall performance of the system [84]. It can be obtained by combining Equations (3.2) and (3.3) as:

$$\eta_{PVT} = \eta_{th} + \eta_{el} = \frac{E_{dc} + E_{th}}{A_m \times G_p} \quad (3.5)$$

Depending on the available data and desired level of resolution, convectional PV and hybrid PVT systems' efficiencies can be determined on instantaneous, hourly, daily, monthly, and annually bases.

3.3.2 Exergy efficiency and analysis

The exergy analysis is based on the second law of thermodynamics. The overall output exergy (Ex_{out}) from PVT system is expressed as:

$$Ex_{out} = Ex_{th} + Ex_{el}, \quad (3.6)$$

where Ex_{el} is the electrical exergy and Ex_{th} is the thermal exergy. Unlike thermal energy, electrical energy is perfectly convertible, and its exergy content can be taken to be same as the energy content. Thus Ex_{el} and Ex_{th} can be expressed in energy terms in kWh as [85]:

$$Ex_{el} = E_{dc}, \quad (3.7)$$

$$Ex_{th} = E_{th} \left(1 - \frac{T_{ref} + 273}{T_o + 273} \right), \quad (3.8)$$

Equation (3.8) shows that the useful product of a PVT thermal collector is the heat extracted from the absorber plate to the fluid and made available at its outlet temperature, T_o . The Carnot Factor, $[1 - (T_{ref} + 273) / (T_o + 273)]$, shows the reference temperature (T_{ref}) at which the exergy content of the thermal power is zero [24]. T_{ref} is generally assumed to be equal to ambient temperature T_a . This is adopted by numerous authors, such as [24] [86]. However, for an uncontrolled environment, T_a frequently fluctuates periodically. Thermal exergy is affected by such fluctuations as it depends on the value of the reference temperature at the moment when heat is delivered [86]. This therefore introduces thermodynamic contradictions because the reference temperature is supposed to be constant. Thus, for this paper, the T_{ref} shall correspond to the monthly minimum ambient temperature $T_{a.min}$ recorded in any given month, as recommended by [86]. Therefore,

$$Ex_{th} = E_{th} \left(1 - \frac{T_{a.min} + 273}{T_o + 273} \right), \quad (3.9)$$

Following the same minimum monthly ambient temperature reference point assumption, the overall exergy efficiency of the PVT could be expressed as [87]:

$$\eta_{ex} = \eta_{el} + \eta_{th} \left(1 - \frac{T_{a.min} + 273}{T_o + 273} \right), \quad (3.10)$$

where η_{ex} is the overall exergy efficiency of the hybrid PVT water-heating system.

3.3.3 Economic performance indicators

The economic assessment is made up of costs and benefits of the system. There are many economic performance indicators used by investment professionals, such as levelized cost of energy (LCOE), net present value (NPV) and simple discounted payback period (PP) [88]. The LCOE is a regularly used metric for evaluating the financial and economic viability of energy technologies [89] [90]. In the case of this study, LCOE is evaluated using NPV techniques. LCOE is the price at which energy must be generated from a specific source to break even over the lifetime of the project. In calculating LCOE, all cost factors such as financing, operation costs, maintenance cost, taxes, support, must be considered. The generalized expression for the LCOE over the life span of an energy system is given as [88] [91]:

$$LCOE = \frac{\text{Net Present value of cash flow}}{\text{Present value of energy}}, \quad (3.11)$$

In exergetic terms, the levelized cost of exergy ($LCOEx$) is defined as

$$LCOEx = \frac{\sum_{t=0}^{b-1} PV_{CF}}{\sum_{t=0}^{n-1} PV_{Ex}}, \quad (3.12)$$

$$PV_{CF} = \frac{C_t}{(1+r)^t}, \quad (3.13)$$

$$PV_{Ex} = \frac{Ex_{pvt,t}}{(1+r)^t}, \quad (3.14)$$

where PV_{CF} is the present value of the cash flow, PV_{Ex} is the present value of the exergy, $Ex_{pvt,t}$ is the annual exergy from the system in year t , b is the economic life of the system, r is the discount rate for cash flow and C_t is the total cost in USD (\$) to the setup in year t . Mathematically, C_t is expressed as

$$C_t = I_t + L_t + M_t + Tx_t - Sp_t, \quad (3.15)$$

where I_t is the total investment expenditure, L_t is the financial loan cost, M_t is total operation and maintenance cost, Tx_t is the total tax paid and Sp_t is the total support and incentives, all in the year t .

Table 3.3 shows a summary of economic parameters and prices of balance of system (BOS) devices used in the setup. Although the cost of mounting rack without labour cost is estimated at 10% of the total cost of Module [92] the same is assumed for the PVT system as well. Also, the operation and maintenance (M_t) for both modules were estimated based on studies by Baumgartner [92]. This includes all labour costs as well as provision of security. It should also be noted that systems were acquired without any financial support.

Table 3.3: Economic parameters

Item/Parameter	Size/Rating	Unit Value or cost (\$)	Unit value Reference
PV	270 W	\$ 254	Actual cost
PVT	1.326 m ²	\$ 392.15/m ²	Actual cost
Mounting rack	% of module cost	10 %	[92]
Inverter Cost, $I_{inv,t}$	Paper 2	\$ 300/kW	Actual cost
Battery bank Cost, $I_{bat,t}$	Paper 2	\$ 160/kWh	Actual cost
Water circulation Pump,	10W	\$ 9/W	Actual cost
Control station	Single unit	\$ 50	[93]
O&M cost per year, M_t	% of module cost	5%/annum	Estimated [92]
Storage tank with heat exchanger	100L	\$ 1.5/Liter	Actual cost
Average Electricity tariff for residential users in Ghana	Average	\$ 0.12/kWh	[94]
Discount rate, r (Dec. 2020)	Return on savings	5%	[95]
Financial support package, Sp_t	% of module cost	0%	Actual situation
Exchange rate (02.07.2021)	\$/GH	5.76	[96]

4 Results and discussion

The findings of this study have been presented in **Paper 1**, **Paper 2** and **Paper 3**. **Paper 1** investigated the influence of meteorological conditions on general energy output and performance indicators, including efficiencies, while **Paper 3** assessed the detailed influence of flowrate configurations of heat extraction fluid on PVT performance. **Paper 2** studied the economic feasibilities of the PVT for its projected life span in the installed environment.

4.1 Climatic effects on performance

The electrical energy efficiency of any PV system is directly related to its cells temperature. **Paper1** studied the influence of the climatic factors (irradiance, ambient temperature and wind velocity) on the temperature of the PVT and PV modules. The average daytime temperatures of the PV module were relatively higher than average PVT module temperatures, ranging between 1.3% to 6.9% higher [83]. Table 4.1 details effects of climatic factors on module temperatures.

Table 4.1: A summary of weather data and module temperatures

Month	Ambient Conditions			Average Daily T_{cell}	
	G_p kWh/m ² /d ay	T_a °C	w m/s	PV °C	PVT °C
January	4.49	30.57	0.56	42.26	40.21
February	4.39	30.86	0.60	42.87	40.69
March	4.90	30.94	0.73	44.22	41.19
April	4.72	30.67	0.75	43.60	40.98
May	4.44	29.88	0.75	41.65	39.33
June	3.67	28.08	0.80	37.87	36.38
July	2.90	26.79	0.81	34.69	34.01
August	2.82	26.62	0.93	34.62	34.17
September	3.20	27.31	0.74	37.16	35.97
October	3.94	28.00	0.78	40.08	38.08
November	4.90	29.91	0.71	43.65	40.80
December	4.25	30.10	0.71	42.58	39.74

PV cells temperature are directly linked to their efficiency (Equation 3.1). An advantage of the PVT over the PV is the cooling effect of the working fluid on the cells. Following

that, in the case of the PVT module, **Paper 3** has shown that increasing mass flowrate of the water (m_w) reduced its temperature non-linearly until such a value ($m_w = \sim 0.082$ kg/s in this case) that any further increase did not result in significant changes in T_c for a specific irradiance. For instance, the T_c significantly reduced by almost 11.3% from 60.3 °C to 53.4 °C for m_w variation from 0.025 – 0.067 kg/s at an irradiance of 900 W/m² [97].

4.2 Energy and Exergy Efficiency of modules

Paper 1 assessed the energetic efficiencies of the modules based on their output energies. Rated electrical efficiencies (DC) for PV and PVT are 16.6% and 15.1% respectively, whereas zero loss thermal efficiency of the PVT thermal collector is 48.0 %, as shown in Table 3.1 for STC. However, in reality, there are significant variations in instantaneous efficiencies calculated from input and output energies from modules installed in uncontrolled environments, which are predominantly lower than values measured at STC. For example, **Paper 1** has shown that the annual average daily electrical efficiencies for the PV and PVT modules were 12.1 % and 10.8 %, whereas the average efficiency of the thermal collector was 36.3 % [83].

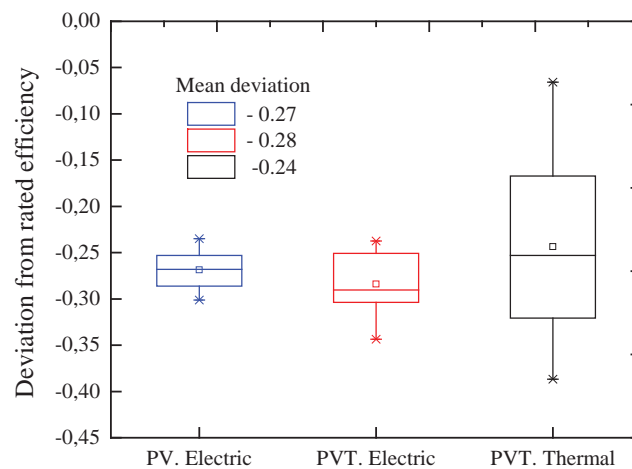


Figure 4.1: Range of deviation of instantaneous energy efficiencies from rated efficiencies at STC

Figure 4.1 shows the range of deviations of instantaneous efficiencies of modules, installed in uncontrolled environment, from rated efficiencies. It could be seen that the mean deviations of the electrical efficiencies for the PV and PVT modules are -26.9 % and -28.3% respectively, whereas the thermal efficiency of the PVT system deviated by -24.3%. This means that although the instantaneous thermal efficiencies for the PVT had wider range variation of 29.4% to 44.8% (**Paper 1** [83]) it recorded the lowest mean

deviation from its rated efficiency. Also, the PVT's instantaneous electrical efficiencies recorded the highest mean deviation from rated efficiency, which is not very different from what was recorded from the PV module. This however means that, the cooling of the PVT cells did not translate directly into efficiency improvement, as compared to the PV cells.

It has also been shown in **Paper 3** that, in exergy terms, the commercial PVT only began to perform better than the conventional PV at higher irradiance (i.e., $\sim 790 \text{ W/m}^2$ in this case) as could be seen from Figure 4.2. However, whereas the PVT seemed to show a relatively stable exergy efficiency with increase in G_p , the PV suffered a decrease in exergy efficiency due to the debilitating effect of higher T_c in the absence of any active cooling. This observation about stability of the PVT exergy efficiency is only true at a specific mass flowrate ($m_w = 0.033 \text{ kg/s}$).

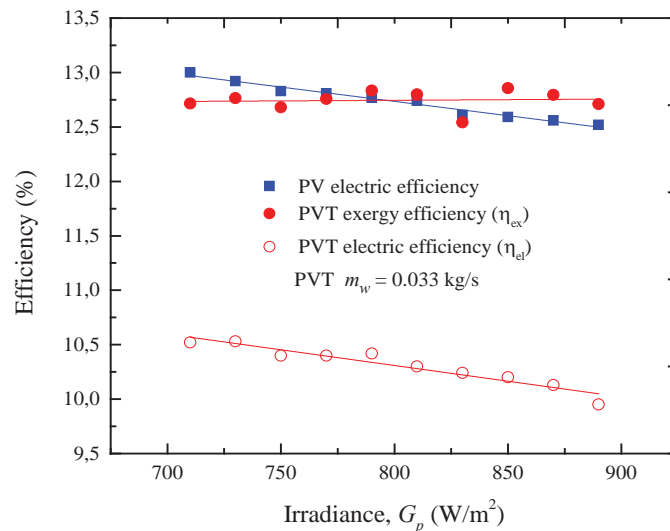


Figure 4.2: Exergy comparison between the conventional PV and the commercial PVT at manufacturer's recommended mass flowrate of 0.033 kg/s

4.3 Long term energy and exergy performance

For the purpose of this analysis, the water circulation through the thermal system of the commercial PVT has been set at manufactures recommended mass flowrate of 0.033 kg/s (2 L/min). The estimated gross annual average outputs from the PVT module for the 25-year economic period are 170.85 kWh/m^2 and 519.69 kWh/m^2 and 377.15 kWh/m^2 for electrical energy (E_{dc}), thermal energy (E_{th}) and total exergy (Ex_{out}) respectively. In the case of the PV module, gross annual average electrical energy output is estimated at $192.58 \text{ kWh/m}^2/\text{annum}$ for the period, which is the same as its exergy (see Equation 3.7).

Paper 2 presented analytical models in a comparative energy and exergy study over a 25-year lifetime of the PVT and PV subsystems. Both subsystems have been modeled with TRNSYS for their economic life-cycle projections based on field measured data. The degradation rate of PVT module and PV module outputs were predicted based on manufacturer warranty information for the modules and measured data, including exergy performance. As could be seen from Figure 4.3, the PV module and PVT module output exergies are estimated to degenerate by 12.8 % and 11.3 % respectively at the end of the 25-year period of continuous exposure. This translates to approximately 6.1% of total exergy lost for each module over the period of study.

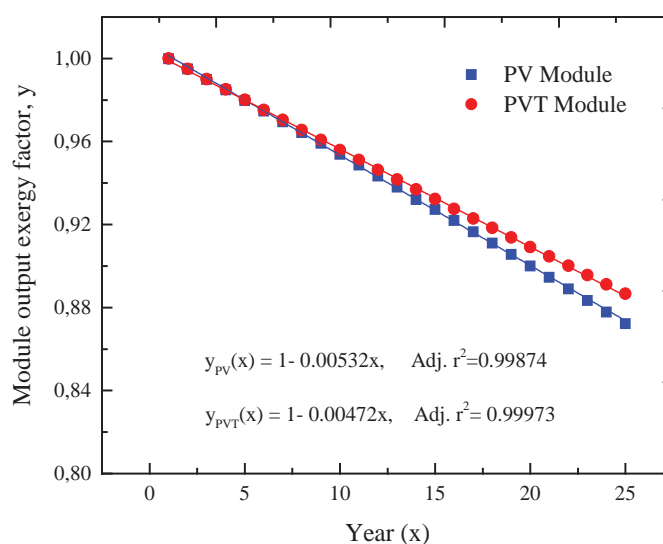


Figure 4.3: Projected exergy output from PV and PVT modules over life span.

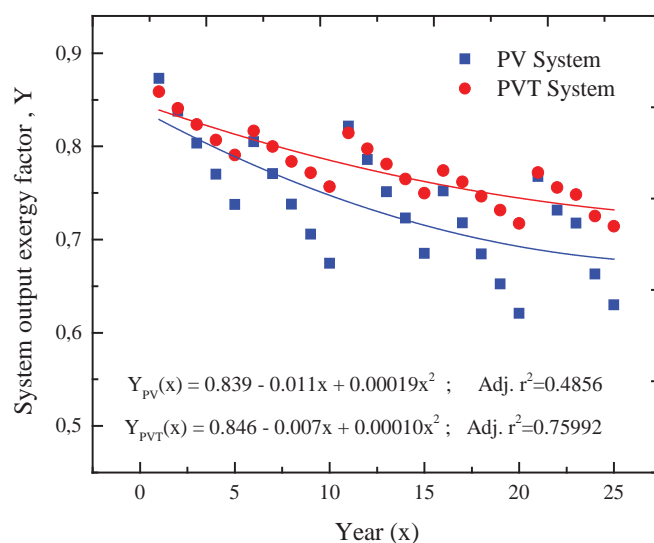


Figure 4.4: Effect of system losses on net exergy output over the years of study.

However, in reality, BOS components contribute to losses in energy transition from modules to load. Figure 4.4 shows that for the period of study, the average net exergy output from the commercial PVT system degenerates curvilinearly from approximately 84.6% to 73.3%, as against 83.9% to 68.3% for the PV system. Thus, the exergy degeneration rate of the commercial PVT is lower than recorded for the conventional PV. The non-linear variation of average percentage of available exergy could be attributed to occasional replacements of BOS devices, as they reached their end of useful life within the study period.

4.4 Economic performance

The economic evaluation of the PV and PVT systems are based on a reference scenario described in **Paper 2** with battery storage capacity in full use ($\beta_t = 1$) at default input parameters ($G_p = 4.5 \text{ kWh/m}^2/\text{day}$, $r = 0.05$, O&M = 5% of module cost, and $Sp_t = 0$) for the 25-year project lifecycle. **Paper 2** also introduces levelized cost of exergy ($LCOEx$) as an economic parameter for fairer economic comparison between the commercial PVT and conventional PV.

One main barrier or concern for the use of renewable energy technology is their high investment cost, with a chunk of it required upfront. For the reference scenario, the net present value of life cycle cashflow (PV_{CF}) per unit area for the PV and PVT sub-systems were respectively \$ 1083/m² and \$ 1665/m². Thus, as expected, the running cost of the commercial PVT system has been generally higher than the conventional PV system. Upfront cost amounted to 58.5% and 68.6% of the net PV_{CF} for the PV and PVT systems respectively. Thus, it requires approximately 80% more upfront cost for setting up the conventional PV-system/m² to setup the commercial PVT-system/m² [98].

The cost of exergy produced from the PVT system (\$ 0.33/kWh) is however generally cheaper than that from the PV system (0.45/kWh) but more expensive than residential tariffs for grid power in Ghana (i.e., \$ 0.06-0.16/kWh, depending on the units of electricity consumed per month [94]). However, for a scenario where the modules are freely acquired through support policies like the National Rooftop Solar Programme [99] and installed without any batteries, the PV system has achieved grid parity in all regions (\$

0.06 - 0.13/kWh) in Ghana, whereas the *LCOEx* for PVT (\$ 0.09 – 0.19 kWh) has compared favorably with tariffs in regions with daily peak sun hours > 3.65 h.

4.5 In comparison with conventional PV systems

Unlike PVTs, conventional PVs are already one of the leading products in the global renewable energy charge. For the commercial PVT to compete well with the conventional systems, the cooling effect on the cells should translate into both electrical energy and thermal energy gains. This calls for alternative design and improvement of the commercial systems. The most common thermal absorber in PVT technology is the tube and sheet design [24] [83] [30]. However, some alternative absorber designs in literature with encouraging performance include spiral flow absorber [33], aluminium-alloy flat box with rectangular channel absorber [35], and serpentine channel absorber [100]. The use of nanofluid technology for heat transfer has also been reported to improve both thermal and electrical energy performance of the PVT [101].

5 Conclusions

The primary aim of this research was to make an original scientific contribution to the subject of real-life performance of a commercial PVT in an uncontrolled environment in West-Africa, by studying a system installed in a Ghanaian environment in comparison with a conventional PV system. Like any solar system, climatic conditions are key to the performance of the PVT collectors. However, although some studies on operational performance of solar PV modules in Ghana can be found in the open literature (e.g. [46] [21] [102]), this experimental study has been the first known attempt to assess a commercial PVT module's real-life performance in the West Africa sub-region. Moreover, for the first time, this research has attempted a comparative study between the two technologies (PV and PVT) in Ghana.

In relation to the research objectives, the major conclusions of the study are presented below:

- The average daytime temperatures of the PVT cells were relatively lower than average PV cells, ranging between 1.3% to 6.9% lower. However, the relatively colder PVT cells did not translate directly into electric efficiency improvement, as compared to convention PV cells. This means that, in terms of electrical energy production, although the commercial PVT operated at lower cell temperatures, its electrical efficiency remained lower than that of the conventional PV at all times.
- In exergy efficiency terms the commercial PVT, operated at manufacturer's recommended mass flowrate, performs better than the conventional PV only when irradiance is beyond a specific higher value ($\sim 790 \text{ W/m}^2$ in this case). Whereas the PVT's exergy efficiency remains constant with increasing irradiance, the PV's exergy efficiency reduces linearly from higher to lower values, in comparison with the PVT's.
- In terms of technical performance, the gross annual average exergy outputs in their life-cycles are 192.58 kWh/m^2 and 377.15 kWh/m^2 respectively measured from the PV and PVT systems.
- The rate of degradation of output exergy due to ageing was projected to be lower in the commercial PVT module than the conventional PV module. This has been

estimated to reach 11.3 % and 12.8 % respectively for the PVT and PV modules in their estimated 25year economic life, which translates into approximately 6.1 % of total exergy losses for each module over the period. Also, whereas the output losses of the PVT system increased curvilinearly from 15.4% to 26.7% over its economic life, that of the PV system increased from 16.1% to 31.7%.

- For complete standalone systems (configured with battery and inverter), the net present value of life cycle cashflow (PV_{CF}) per unit area for the PV and PVT systems are estimated at \$ 1083 and \$ 1665. Upfront costs amounted to 58.5% and 68.6% of PV_{CF} for setting up the PV and PVT systems respectively. The study estimated the upfront cost to be approximately twice what was required in setting up the conventional PV system to setup the same surface area of the commercial PVT system.
- The study introduced the use of levelized cost of exergy ($LCOEx$) as an economic parameter, instead of energy, for a fairer cost comparison of net energy from PV and PVT systems. The cost of exergy produced from the PVT system is averagely 36.4% cheaper than from the PV system, but more expensive than residential tariffs for grid power in Ghana. However, when installed without batteries, the PV's exergy becomes cheaper.

6 Limitations of work, future studies and engineering direction.

Following the conclusions above, it is possible to state that the current thesis has successfully assessed the field performance of a commercial PVT in the context of the listed objectives. While the methods adopted in this thesis accounted for significant sources of uncertainties, some issues could be recommended as subjects for further investigation and to potentially minimize uncertainties in the assessments:

- The results highlight the importance of climatic conditions. The reliability of climate impact assessments depends on the quality and duration of the weather data. However, climatic related impact assessments were based on measured weather data over a single year. Since weather changes are very unpredictable, such short-term data may not be enough to draw accurate conclusions. Further studies on impact assessment should be based on long term weather data collected at installation site.
- Also, the prediction of long-term performance of the PVT and PV modules were based on analytical models and a TRNSYS model based on the same short-term measured data. Since this study is the first of its kind in such an environment, with unique weather conditions like harmattan, there is no evidence in literature to ascertain the veracity of the models in the long term. Thus, further research based on long term observations is necessary to validate or correct existing models and to accurately predict long term performance.
- The study was also based on only mono-crystalline silicon technology for both PV and PVT modules. This was because of non-availability of commercial PVT products on the Ghanaian market. The only available source in Europe ready to export to Ghana had only crystalline silicon modules in stock. While the results may have been based on modules from one technology and manufacturer, yet it provides stronger reference for comparison with other products across other geo-climatic zones. However, future works could expand scope to include other PV and PVT technologies from different manufactures and technologies.
- Extreme test conditions are rare to achieve in real life situations. Well-equipped simulation solar labs with measuring instrument and weather conditioning

possibilities should be established for future works to generate data in support of solar industry in Ghana. With that in place, the PVT's behavior in such extremities could be assessed in the future.

- A lifecycle assessment is a comprehensive tool for quantifying the lifetime environmental impacts of energy systems. However, the study focused on the productive life of the modules without considering environmental impacts. Future studies into lifecycle assessment of the PVT and PV modules will evaluate adverse impacts from cradle-to-grave; starting from inputs (raw materials & energy) and production outflows (emissions, waste & product), transportation, use, decommissioning and management as waste.
- The study was premised on the reported high temperatures of PVs installed in that environment. The PVT was therefore investigated as an alternative technology, without considering stand-alone thermal systems. A future study could assess the performance PVT against both PV's and solar thermal systems in that environment

For the commercial PVT to compete well with the conventional systems, the cooling effect on the cells should translate into both electrical energy and thermal energy gains. Its electrical efficiency was generally lower than that of the conventional PV system. Different assembling techniques and materials could be used to improve the PVT electrical efficiency. Also, cheaper, and more efficient batteries with longer charge/discharge lifecycles could significantly improve both techno and economic performance of stand-alone PV/PVT systems. This observation is, however, based on mc-Si technology and specific commercial manufacturer's design, may not be generalized for all other PV/PVT technologies.

References

- [1] "WHO," 21 May 2019. [Online]. Available: <https://www.who.int/news/item/21-05-2019-more-people-have-access-to-electricity-than-ever-before-but-world-is-falling-short-of-sustainable-energy-goals>. [Accessed 3 February 2021].
- [2] "SDG7: Data and Projections," [Online]. Available: <https://www.iea.org/reports/sdg7-data-and-projections/access-to-electricity>. [Accessed 22 March 2021].
- [3] "WHO: Household air pollution and health," 8 May 2018. [Online]. Available: <https://www.who.int/en/news-room/fact-sheets/detail/household-air-pollution-and-health>. [Accessed 10 February 2021].
- [4] "WHO Malaria," 30 November 2020. [Online]. Available: <https://www.who.int/en/news-room/fact-sheets/detail/malaria>. [Accessed 30 November 2021].
- [5] "WHO Tuberculosis," 14 October 2020. [Online]. Available: <https://www.who.int/en/news-room/fact-sheets/detail/tuberculosis>. [Accessed 10 February 2021].
- [6] "BP Energy Outlook," 2017. [Online]. Available: <https://www.bp.com/content/dam/bp/business-sites/en/global/corporate/pdfs/energy-economics/energy-outlook/bp-energy-outlook-2017.pdf>. [Accessed 20 January 2021].
- [7] "International Energy Outlook 2017," 14 September 2017. [Online]. Available: [https://www.eia.gov/outlooks/ieo/pdf/0484\(2017\).pdf](https://www.eia.gov/outlooks/ieo/pdf/0484(2017).pdf). [Accessed 25 11 2020].
- [8] C. Rajoria, S. Agrawal and G. Tiwari, "Overall thermal energy and exergy analysis of hybrid photovoltaic thermal array," *Solar Energy*, vol. 86, pp. 1531-1538, 2012.
- [9] F. Ghani, M. Duke and C. J.K., "Estimation of photovoltaic conversion efficiency of a building integrated photovoltaic/thermal (BIPV/T) collector array using an artificial neural network," *Solar Energy*, vol. 86, pp. 3378-3387, 2012.
- [10] "Paris Agreement," UN, 2015. [Online]. Available: https://unfccc.int/sites/default/files/english_paris_agreement.pdf. [Accessed 6 January 2021].
- [11] "UN Treaty Collection," UN, 12 December 2015. [Online]. Available: https://treaties.un.org/pages/ViewDetails.aspx?src=TREATY&mtdsg_no=XXVII-7-d&chapter=27&clang=_en. [Accessed 6 January 2021].
- [12] "REN21," June 2020. [Online]. Available: https://www.ren21.net/wp-content/uploads/2019/05/gsr_2020_full_report_en.pdf. [Accessed 14 12 2020].
- [13] "Sustainable Energy for All," [Online]. Available: http://www.se4all.org/sites/default/files/1/2013/09/SG_Sustainable_Energy_for_All_vision_final_clean.pdf. [Accessed 3 February 2021].
- [14] M. Kibati and V. G. Desroches, "Power For All," 16 November 2018. [Online]. Available: <https://www.powerforall.org/insights/africa/electrifying-africas-labor-market>. [Accessed 9 February 2021].
- [15] "IRENA," 2020. [Online]. Available: <https://www.irena.org/publications/2019/Jun/Renewable-Energy-and-Jobs-Annual-Review-2019>. [Accessed 10 February 2021].

- [16] S. Baljit, C. H.Y and S. K, "Review of building integrated applications of photovoltaic and solar thermal systems," *Journal of Cleaner Production*, vol. 137, pp. 677-689, 2016.
- [17] H. Zondag, "Flat-plate PV-Thermal collectors and systems: A review," *Ren. and Sust. Energy Reviews*, vol. 12, no. 4, pp. 891-959, 2008.
- [18] I. Gurracino, C. Markides, A. Mellor and N. Ekins-Daukes, "Dynamic coupled thermal and electrical modelling of sheet and tube hybrid photovoltaic/ thermal (PVT) collectors," *Appl. Therm. Eng.*, vol. 101, pp. 778-795, 2016.
- [19] C. Good, "Environmental impact assessment of hybrid photovoltaic-thermal (PV/T) Systems – A review.," *Renewable and sustainable energy reviews*, vol. 55, pp. 234-239, 2016.
- [20] H. Amal, E. H. Hicham, L. Thiery, R. Mohamad and K. Mahmoud, "Review on photovoltaic/thermal hybrid solar collectors: Classifications, T applications and new systems," *Solar Energy*, vol. 207, pp. 1321-1347, 2020.
- [21] D. A. Quansah, M. S. Adaramola and G. K. Appiah, "Performance analysis of different grid-connected solar photovoltaic (PV) system technologies with combined capacity of 20 kW located in humid tropical climate," *International Journal of Hydrogen Energy*, vol. 42 , pp. 4626 - 4635, 2017.
- [22] M. Fuentes, M. Vivar, J. de la Cassa and J. Aguilera, "An experimental comparison between commercial hybrid PV-T and simple PV systems intended for BIPV," *Renewable and Sustainable Energy Reviews*, vol. 93, pp. 110-120, 2018.
- [23] T. Chow, "A review on photovoltaic/thermal hybrid solar technology," *Applied Energy*, vol. 87, pp. 365-379, 2010.
- [24] M. Fuentes, M. Vivar, J. de la Casa and J. Aguilera, "An experimental comparison between commercial hybrid PV-T and simple PV systems intended for BIPV," *Renewable and Sustainable Energy Reviews*, vol. 93, pp. 110-120, 2018.
- [25] C. de Keizer, M. de Jong, T. Mendes, M. Katiyar, W. Folkerts, C. Rindt and H. Zondag, "Evaluating the thermal and electrical performance of several uncovered PVT collectors with a field test," *Energy Procedia*, vol. 91, pp. 20-26, 2016.
- [26] O. Rejeb, H. Dhaou and A. Jemni, "A numerical investigation of a photovoltaic thermal (PV/T) collector," *Renew. Energy*, vol. 77, pp. 43-50, 2015.
- [27] N. Aste, C. del Pero and F. Leonforte, "Water flat plate PV-thermal collectors: A review," *Solar Energy*, vol. 102, pp. 98-115, 2014.
- [28] M. Lämmle, A. Olivia, M. Hermann, K. Kramer and W. Kramer, "PVT collector technologies in solar thermal systems. A systematic assessment of electrical and thermal yields with the novel characteristic temperature approach," *Solar Energy*, vol. 155, pp. 867-879, 2017.
- [29] A. S. Kalogirou, "Use of TRNSYS for modelling and simulation of a hybrid pv–thermal solar system for Cyprus," *Renewable Energy*, vol. 23, no. 2, pp. 247-260, 2001.
- [30] I. Guarracino, J. Freeman, A. Ramos, A. S. Kalogirou, J. N. Ekins-Daukes and N. C. Markides, "Systematic testing of hybrid PV-thermal (PVT) solar collectors in steady-state and dynamic outdoor conditions," *Applied Energy*, vol. 240, pp. 1014-1030, 2019.
- [31] P. Dupeyrat, C. Ménézo, M. Rommel and H. Henning, "Efficient single glazed flat plate photovoltaic–thermal hybrid collector for domestic hot water system," *Sol. Energy*, vol. 85, pp. 1457-1468, 2011.

- [32] S. Kalogirou and Y. Tripanagnostopoulos, "Industrial application of PV/T solar energy systems," *Applied Thermal Engineering*, vol. 27, p. 1259–1270, 2007.
- [33] A. Fudholi, S. Kamaruzzaman, H. M. Yazdi, H. M. Ruslan, A. Ibrahim and A. H. Kazem, "Performance analysis of photovoltaic thermal (PVT) water collectors," *Energy Conversion and Management*, vol. 78, pp. 641-651, 2014.
- [34] B. Huang, T. Lin, W. Hung and F. Sun, "Performance evaluation of solar photovoltaic/thermal systems," *Sol. Energy*, vol. 70, pp. 443-448, 2001.
- [35] T. Chow, J. Ji and W. He, "Photovoltaic-Thermal Collector System for Domestic Application," *J. Sol. Energy Eng.*, vol. 129, no. 2, pp. 205-209, 2007.
- [36] W. He, T. Chow, J. Ji, J. Lu, G. Pei and L. Chan, "Hybrid photovoltaic and thermal solar-collector designed for natural circulation of water," *Appl. Energy*, vol. 83, pp. 199-210, 2006.
- [37] J. Ji, J. Han, T. Chow, H. Yi, J. Lu, W. He and W. Sun, "Effect of fluid flow and packing factor on energy performance of a wall-mounted hybrid photovoltaic/water-heating collector system.," *Energy Build*, vol. 38, pp. 1380-1387, 2006.
- [38] M. Hazami, A. Ali Riahi, F. Mehdaoui, O. Omeima Nouicer and A. Farhat, "Energetic and exergetic performances analysis of a PV/T (photovoltaic thermal) solar system tested and simulated under Tunisian (North Africa) climatic conditions," *Energy 2016*, vol. 10715, pp. 78-94, 2016.
- [39] M. Abdulkadir and S. Muhammad, "Design and construction of a thermosiphonic solar photovoltaic: Thermal water heating system for sustainable development in temperate regions of Africa.," *J. Altern. Energy Sources Technol*, vol. 8, pp. 1-8, 2017.
- [40] J. Siecker, K. Kusakan and B. Numbi, "Optimal switching control of PV/T systems with energy storage using forced water circulation: Case of South Africa," *J. Energy Storage*, vol. 20, pp. 264-278, 2018.
- [41] A. Oyieke and F. Inambao, "Performance characterisation of a hybrid flat-plate vacuum insulated photovoltaic/thermal solar power module in subtropical climate," *Int. J. Photoenergy*, no. 2, pp. 1-15, 2016.
- [42] O. Apuko and Inambao, "Simulation and performance evaluation of a vacuum insulated hybrid solar photovoltaic/thermal power module for domestic applications in South Africa," *TMC Acad. J.*, no. 9, pp. 1-19, 2015.
- [43] W. Sawadogo, B. Abiodun and E. Okogbue, "Impacts of global warming on photovoltaic power generation over West Africa," *Renew. Energy*, vol. 151, pp. 263-277, 2020.
- [44] S. Meunier, M. Heinrich, L. Quéval, J. Cherni, L. Vido, A. Darga, P. Dessante, B. Multon, P. Kitanidis and C. Marchand, "A validated model of a photovoltaic water pumping system for o-grid rural communities," *Appl. Energy*, vol. 241, pp. 580-591, 2019.
- [45] D. Akinyele, O. Babatunde, C. Monyei, L. Olatomiwa, A. Okediji, D. Ighravwe, O. Abiodun, M. Onasanya and K. Temikotan, "Possibility of solar thermal power generation technologies in Nigeria: Challenges and policy directions.," *Renew. Energy Focus*, vol. 29, pp. 24-41, 2019.
- [46] F. Nyarko, G. Takyi, E. Amalu and M. Adaramola, "Generating temperature cycle profile from in-situ climatic condition for accurate prediction of thermo-mechanical degradation of c-Si photovoltaic module," *Eng. Sci. Technology Int. J.*, vol. 22, pp. 502-514, 2019.

- [47] D. Quansah and M. Adaramola, "Assessment of early degradation and performance loss in five co-located solar photovoltaic module technologies installed in Ghana using performance ratio time-series regression.," *Renew. Energy*, vol. 131, pp. 900-910, 2019.
- [48] A. Yushchenko, A. de Bono, B. Chatenoux, M. Patel and M. Ray, "GIS-based assessment of photovoltaic (PV) and concentrated solar power (CSP) generation potential in West Africa," *Renew. Sustain. Energy Rev*, no. 81, pp. 2088-2103, 2018.
- [49] M. Simo-Tagne, M. Ndukwu, A. Zoulalian, L. Bennamoun, F. Kifani-Sahban and Y. Rogaume, "Numerical analysis and validation of a natural convection mix-mode solar dryer for drying red chilli under variable conditions," *Renew. Energy*, vol. 151, pp. 659-673, 2020.
- [50] O. Ogunmodimu and Okoroigwe, "E.C. Solar thermal electricity in Nigeria: Prospects and challenges," *Energy Policy*, vol. 128, pp. 440-448, 2019.
- [51] Y. Seshie, K. N'Tsoukpoe, P. Neveu, Y. Coulibaly and Y. Azoumah, "Small scale concentrating solar plants for rural electrification.," *Renew. Sustain. Energy Rev.*, vol. 90, pp. 195-209, 2018.
- [52] M. Herrando, N. C. Markides and K. Hellgardt, "A UK-based assessment of hybrid PV and solar-thermal systems for domestic heating and power: System performance," *Applied Energy*, vol. 122, pp. 288-309, 2014.
- [53] M. Herrando and C. N. Markides, "Hybrid PV and solar-thermal systems for domestic heat and power provision in the UK: Techno-economic considerations," vol. 161, pp. 512-532, 2016.
- [54] S. Tselepis and Y. Tripanagnostopoulos, "Economic analysis of hybrid photovoltaic/thermal solar systems and comparison with standard PV modules," in *Proceedings of the International Conference On PV in Europe*, 2001.
- [55] [Online]. Available: [http://energycom.gov.gh/files/Solar%20Data%20-%20final\(1\).pdf](http://energycom.gov.gh/files/Solar%20Data%20-%20final(1).pdf). [Accessed 10 November 2020].
- [56] "SHC TASK 60," Task 60, February 2019. [Online]. Available: <https://task60.iea-shc.org/highlights>. [Accessed 20 September 2020].
- [57] S. Arno, J. Klaus, I. Olindo, V. S. René and M. Zeman, *Solar Energy: The physics and engineering of photovoltaic conversion technologies and systems*, Cambridge: UIT Cambridge Ltd, 2016.
- [58] J. C. C., *Physics of Solar Energy*, USA: John Wiley & Sons, Inc, 2011.
- [59] A. B. Waheed, "A review on solar cells from Si-single crystals to porous materials and quantum dots," *J. of Adv. Research*, vol. 6, no. 2, pp. 123-132, 2015.
- [60] W. Shockley, "The Theory of p-n Junctions in Semiconductors and p-n Junction Transistors.," *Bell Syst. Tech.*, vol. 28, pp. 435-489, 1949.
- [61] G. Martin, D. Ewan, H.-E. Jochen, Y. Masahiro, K. Nikos and H. Xiaojing, "Solar cell efficiency tables (version 57)," *Progress in Photovoltaics*, 2020.
- [62] B. H. Mohammed, D. Ali, C. M. Keitumetse, A. Lana and A. Niaz, "Solar energy—A look into power generation, challenges, and a solar-powered future," *Int. Journ. of Energy research*, 2018.
- [63] J. Cubas, S. Pindado and C. d. Manuel, "Explicit Expressions for Solar Panel Equivalent Circuit Parameters Based on Analytical Formulation and the Lambert W-Function," *Energies*, vol. 7, pp. 4098-4115, 2014.

- [64] A. Cuevas, "The Recombination Parameter J_0 ," *Energy Procedia*, vol. 55, pp. 53-62, 2014.
- [65] K. Kennerud, "Analysis of Performance Degradation in CdS Solar Cells," *IEEE Trans. Aerosp. Electron. Syst.*, Vols. AES-5, pp. 912-917, 1969.
- [66] C. Javier, P. Santiago and V. Marta, "On the analytical approach for modeling photovoltaic systems behavior," *Journal of Power Sources*, vol. 247, pp. 467-474, 2014.
- [67] R. Ewa, "Performance Analysis of a Photovoltaic-Thermal Integrated System," *Int. Journal of Photoenergy*, vol. 2009, 2009.
- [68] "Everything about solar energy," 4 August 2015. [Online]. Available: <http://energyprofessionalsymposium.com/?p=9811>. [Accessed 6 January 2022].
- [69] D. Evans, "Simplified method for predicting PV array output," *Solar Energy*, vol. 27, pp. 555-560, 1981.
- [70] J. Duffie and W. Beckman, *Solar engineering of thermal processes*. 2nd ed., New York: John Wiley and Sons, Inc., 1991.
- [71] M. Kutz, *Heat transfer Calculations*, McGraw-Hill Companies, 2004.
- [72] A. K. Soteris, *Solar Energy Engineering Processes and Systems (2nd Edition)*, Elsevier, 2014.
- [73] H. Hottel and A. Whiller, "Evaluation of flat-plate solar collector performance, In: The conference on the Use of Solar Energy," *The Scientific Basis*, vol. 2, no. 1, pp. 74-104, 1958.
- [74] A. James, D. Zahir, S. Sinisa and M. Lascelle, "Performance testing of thermal and photovoltaic thermal solar collectors," *Energy Science & Engineering*, vol. 3, no. 4, pp. 310-326, 2015.
- [75] S. Klein, "Calculation of Flat-Plate Loss Coefficients," *Solar Energy*, vol. 17, no. 79, 1975.
- [76] W. Andy, "Whole building design guide," 11 November 2016. [Online]. Available: <https://www.wbdg.org/resources/solar-water-heating>. [Accessed 20 Jan 2022].
- [77] J. Stulz and L. Wen, "Thermal Performance Testing and Analysis of Photovoltaic Modules in Natural Sunlight," 1977.
- [78] D. Jelena, b. SvetlanaI and D. Zorica, "Experimental design application and interpretation in pharmaceutical technology," *Computer-Aided Application in Pharmaceutical Technology*, pp. 31-56, 2013.
- [79] "International standard ISO /FDIS 9806," 2013. [Online]. Available: www.iso.org. [Accessed 2021].
- [80] "Solimpeks solar energy corpl," [Online]. Available: <https://solimpeks.com>. [Accessed 20 January 2022].
- [81] "World Atlas," 9 November 2020. [Online]. Available: <https://www.worldatlas.com/maps/ghana>. [Accessed 10 February 2021].
- [82] M. Peel, Finlayson and M. T.A, "Updated world map of the Koppen-Geiger climate classification," *Hydrology and Earth System Sciences Discussions*, pp. 439-473, 2007.
- [83] S. Abdul-Ganiyu, A. D. Quansah, W. E. Ramde, R. Seidu and A. S. Muiyiwa, "Investigation of Solar Photovoltaic-Thermal (PVT) and Solar Photovoltaic (PV) Performance: A Case Study in Ghana," *energies*, 2020.

- [84] E. Radziemska, "Performance Analysis of a Photovoltaic-Thermal Integrated System," *International Journal of Photoenergy*, vol. 2009, 2009.
- [85] M. Bosanac, B. Sørensen, I. Katic, H. Sørensen, B. Nielsen and J. Badran, "Photovoltaic/Thermal Solar Collectors and Their Potential in Denmark," 21 May 2003. [Online]. Available: <https://www.yumpu.com/en/document/read/4467325/photovoltaic-thermal-solar-collectors-and-their-potential-in-denmark>. [Accessed 8 June 2020].
- [86] M. Pons, "On the Reference State for Exergy when Ambient Temperature Fluctuates*," *Int. J of Thermodynamics*, vol. 12, no. 3, pp. 113-121, 2009.
- [87] A. Tiwari and M. Sodha, "Performance evaluation of solar PV/T system: an experimental validation," *Sol Energy*, vol. 80, no. 7, pp. 751-759, 2006.
- [88] Y. Gu, X. Zhang, J. A. Myhren, M. Han, X. Chen and Y. Yuan, "Techno-economic analysis of a solar photovoltaic/thermal (PV/T) concentrator for building application in Sweden using Monte Carlo method," *Energy Conversion and Management*, vol. 165, pp. 8-24, 2018.
- [89] A. D. Quansah, A. S. Muyiwa, E. A. Isaac and K. E. Anto, "An Assessment of Grid-Charged Inverter-Battery Systems for Domestic Applications in Ghana," *Journal of Solar Energy*, 2016.
- [90] D. A. Quansah and M. S. Adaramola, "Economic assessment of a-Si and CIS thin film solar PV technologies in Ghana," *Sustainable Energy Technologies and Assessments*, vol. 18, p. 164–174, 2016.
- [91] C. B. Riggs, R. Biedenharn, C. Dougher, V. Y. Ji, Q. Xu, V. Romanin, S. D. Codd, M. J. Zahler and D. M. Escarra, "Techno-economic analysis of hybrid PV/T systems for process heat using electricity to subsidize the cost of heat," *Applied Energy*, vol. 208, pp. 1370-1378, 2017.
- [92] F. Baumgartner, "Photovoltaic (PV) balance of system components: Basic, performance.," *The Performance of Photovoltaic (PV) Systems Modelling, Measurement and Assessment*, pp. 135-181, 2017.
- [93] "SOLIMPEKS," [Online]. Available: <https://www.solimpeks.com/volther-powervolt-en>. [Accessed 9 February 2021].
- [94] "PURC," 16 December 2021. [Online]. Available: <https://www.purc.com.gh/attachment/642643-20210225110236.pdf>. [Accessed 18 July 2021].
- [95] "Saving Interest Rates," Standard Chartered Bank, [Online]. Available: <https://www.sc.com/gh/save/savings-plus/>. [Accessed 26 July 2021].
- [96] "BOG," 2020. [Online]. Available: <https://www.bog.gov.gh/>. [Accessed 17 July 2021].
- [97] S. Abdul-Ganiyu, A. D. Quansah, W. E. Ramde, R. Seidu and A. S. Muiyiwa, "Flow-rate analysis of a commercial flat-plate water-based PVT system," *Journal of Cleaner Production*, vol. 321, no. JCLP 128985, 2021.
- [98] S. Abdul-Ganiyu, A. D. Quansah, W. E. Ramde, R. Seidu and A. S. Muiyiwa, "Techno-economic analysis of solar photovoltaic (PV) and solar photovoltaic thermal (PVT) systems using exergy analysis," *Sustainable Energy Technologies and Assessments*, vol. 47, no. 101520, October 2021.
- [99] K. F. Appiah, "The National Rooftop Solar Programme," 9 August 2016. [Online]. Available: <http://energycom.gov.gh/files/ROOFTOP%20SOLAR%20PROG->

Presentation%20@%202nd%20Ghana%20Renewable%20Energy%20Fair1.pdf.
[Accessed 10 June 2020].

- [100] J. Allan, Z. Dehouche, S. Stankovic and L. Mauricette, "Performance testing of thermal and photovoltaic thermal solar collectors," *Energy Science & Engineering*, vol. 3, no. 4, pp. 310-326, 2015.
- [101] H. Fayaz, R. Nasrin, N. Rahim and M. Hasanuzzaman, "Energy and exergy analysis of the PVT system: Effect of nanofluid flow rate," *Solar Energy*, vol. 169, pp. 217-230, 2018.
- [102] K. G. Adanu, "Performance of a 268 Wp stand-alone PV system test facility," in *Proceedings of 1994 IEEE 1st World Conference on Photovoltaic Energy Conversion - WCPEC (A Joint Conference of PVSC, PVSEC and PSEC)*, Hawaii, 1994b.

Paper I

Abdul-Ganiyu, S., Quansah, D.A., Ramde, E.W., Seidu, R. & Adaramola, M.S. 2020. Investigation of Solar Photovoltaic-Thermal (PVT) and Solar Photovoltaic (PV) Performance: A Case Study in Ghana. – *Energies* 13(11): 2701. 17 pp.
DOI: [10.3390/en13112701](https://doi.org/10.3390/en13112701)

Paper II

Abdul-Ganiyu, S., Quansah, D.A., Ramde, E.W., Seidu, R. & Adaramola, M.S. 2021. Techno-economic analysis of solar photovoltaic (PV) and solar photovoltaic thermal (PVT) systems using exergy analysis. – *Sustainable Energy Technologies and Assessments* 47: 101520. 12 pp.
DOI: [10.1016/j.seta.2021.101520](https://doi.org/10.1016/j.seta.2021.101520)

Paper III

Abdul-Ganiyu, S., Quansah, D.A., Ramde, E.W., Seidu, R. & Adaramola, M.S. 2021. Study effect of flow rate on flat-plate water-based photovoltaic-thermal (PVT) system performance by analytical technique. – *Journal of Cleaner Production* 321: 128985. 10 pp.
DOI: [10.1016/j.jclepro.2021.128985](https://doi.org/10.1016/j.jclepro.2021.128985)

ISBN: 978-82-575-1862-2
ISSN: 1894-6402



Norwegian University
of Life Sciences

Postboks 5003
NO-1432 Ås, Norway
+47 67 23 00 00
www.nmbu.no